Plasmon-Fano Resonance in Electron Conduction Band Coupled to Single Laser Mode

Dissertation

zur

Erlangung des Doktorgrades (Dr.rer.nat.)

der

Mathematisch-Naturwissenschaftlichen Fakultät

der

Rheinischen Friedrich-Wilhelms-Universität Bonn

vorgelegt von

Jiarong Zheng

aus

Guangdong, V.R.China

Bonn 2009

Angefertigt mit Genehmigung der Mathematisch-Naturwissenschaftlichen
Fakultät der Rheinischen Friedrich-Wilhelms-Universität Bonn

1.Gutachter: Prof. Dr. Johann Kroha

2.Gutachter: Prof. Dr. Herbert Dreiner

Tag der Promotion: 15.01.2010

Erscheinungsjahr: 2010

Abstract

Plasom related physics has been the subject of extensive reserach interests. In this thesis single laser mode coupled to electron conduction band is studied. The system is nonequilibrium. Keldysh Green's function formalism is applied in this problem. We obtain self-consistency equation in Keldysh space. Numerical results are shown for the electron density of states and distribution function. The competition between laser intensity and electron coulumb interaction has also been studied.

Contents

Chapter 1

Introduction

Nowadays the study of plasmon and photonic physics is becoming more and more important. Research progress of these fields can be soon turned into real application in the industry[1, 2, 3, 4]. One of the example is the application in computer technology. Nowadays the chip scale has reached the size as small as nano meter. At this scale, quantum fluctuations will become significant. The electronic circuit would have failed to work properly if it keeps reducing the scale of the chip structure. The neuest CPUs of our computers are produced in the size of some 10 nano meters. It will be very difficult to continue to improve the performance of CPU chip by reducing electronic circuits scale. Thus the performance of electronic circuits is becoming very limited when large amount of digital information need to be processed. It is necessary to find another way out of this. Photonics offers a possible solution to this difficult problem[5]. Communication systems based on optical fibers and photonic circuits[6, 7, 8] offers a plausible solution. The optical interconnects such as fiber optic cables can carry digital data with capacity much greater than that of electronic interconnects. But typical photonic circut components are of micrometer scale, and it is not possible to integrate them into electronic chips. With plasom physics, the electronics and photonics can be combined and work together at nanoscale. This is only one of the perspectives. Plasmons have also been basis of high-resolution lithography and microscopy due to their extremely small wavelengths. In lab environment these applications have been demonstrated successfully.

In general, plasmon physics describes the coupling of photons to electrons unter different geometry. In this thesis, we will work on electron conduction band coupled to a single photon mode. The nonequilibrium Green's function

enable us to introduce a nonequilibrium laser distribution function.

This thesis is organized as follows. In chapter 2, we discuss experimental motivation related to plasmon physics. Chapter gives an overview to plasmon related physics. Chapter 4 introduces the Keldysh Green's function formalism. Chapter 5 focus on our model: electrons coupled to a single laser mode. In chapter 6, numerical implementation is presented. We will discuss results in chapter 7. Chapter 8 gives a summary to this thesis.

Chapter 2

Experimental Motivation

2.1 A Plasmonic Revolution

Nowadays the human being are basically using two ways to tranfport data. The first one is with electronic circuits. But the performance of electronic circuits is now becoming rather limited. This has become evident since the annual increase of the microprocessor clock speed has slowed down, might reach the limit in the short future. The other way is the photonic fiber. They can carry huge amounts of data, but are much bigger in size. Now people are considering a technology combining the advantages of photonics and electronics. The plasmonic is so far a promising candidate. Theoretically, it is possible to design plasmonic components with the same materials used by chipmakers, but with frequency 100,000 times larger than that of microprocessors. The idea is to have a circuit in nanoscale, carries both optical signals and electric currents. Labor experiments are leading to this goal although there is still quite a long way[9, 10, 11, 12].

Difficulty in integrating the optical and electronic circuits are their different sizes. The electronic circuits are usually at the scale of below 100 nm. On the other hand, in photonics circuits the wavelength of light is in the order of 1000 nm. The photonic crystal doesn't help to solve the problem, because the crystal is still too large comparing to electronic.

Surface plasmon is a outstanding candidate who provides the opportunity to confine photons to a very small volume. When photons reach the metal-dielectric interface[13, 14], where a group of electrons is collectively moving back and forth, they are trapped near the surface and interact with the elec-

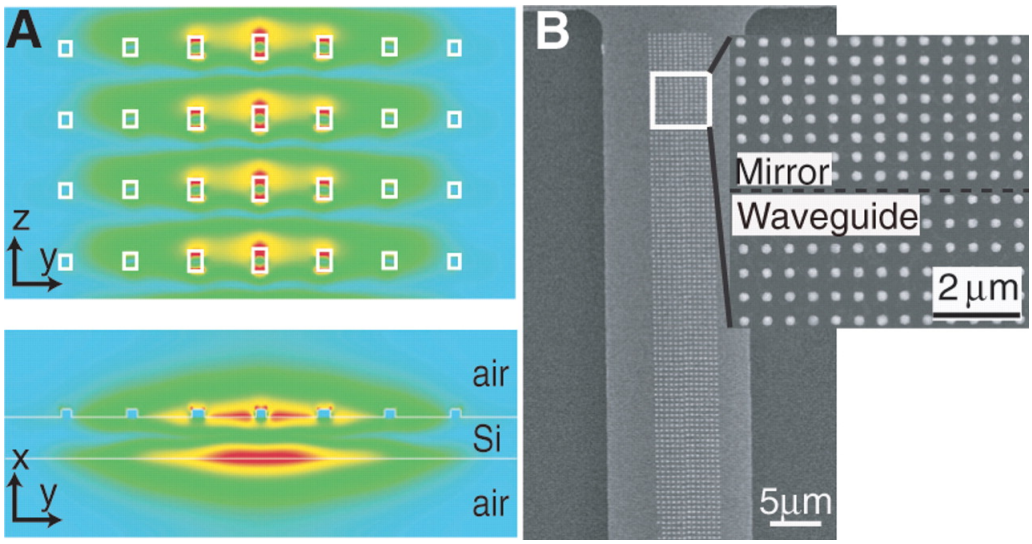

Figure 2.1: Ozbay,Ekmel. Science 311:189-193 (2006)

trons near the surface of metal. Due to the resonant interaction between the photons and electron-charged oscillations, it appears spatially confinement of photons.

The decay length of the surface plasmon is determined by the skin depth[4], about two orders of magnitudes smaller than the wavelength of the light in the air. Thus there is a possibility to apply plasmon to localize and guide the photons in the subwavelength metallic structures.

Therefore plasmonic waveguides are capable of guiding the plasmonic signals in circuits. There are kinds of geometry design to do this. Thin metal dots with finite width are embedded in dieletric so that it forms a plasmonic waveguides. Stefan et al[15] sucessfully demonstrated an effective plasmonic waveguide structure (see Fig2.1). In their experiment, nanoscale gold dots were patterned on a silicon-on-insulator to define the plasmon propagation path (Fig2.1 part A). Figure 2.1B shows the scanning electron micrographs of the fabricated plasmonics waveguides designed for operation at wavelength of 1500 nm. Nanoscale gold dots are assembled on silicon-on-insulator surface. The waveguide structure is not uniform across its width where the size of metal dots is reduced from $80nm \times 80nm$ at the center to $50nm \times 50nm$ at the edges. The light propagation is better concentrate in the middle of the waveguide. Figure 2.1A show a FDTD simulation of the electric field

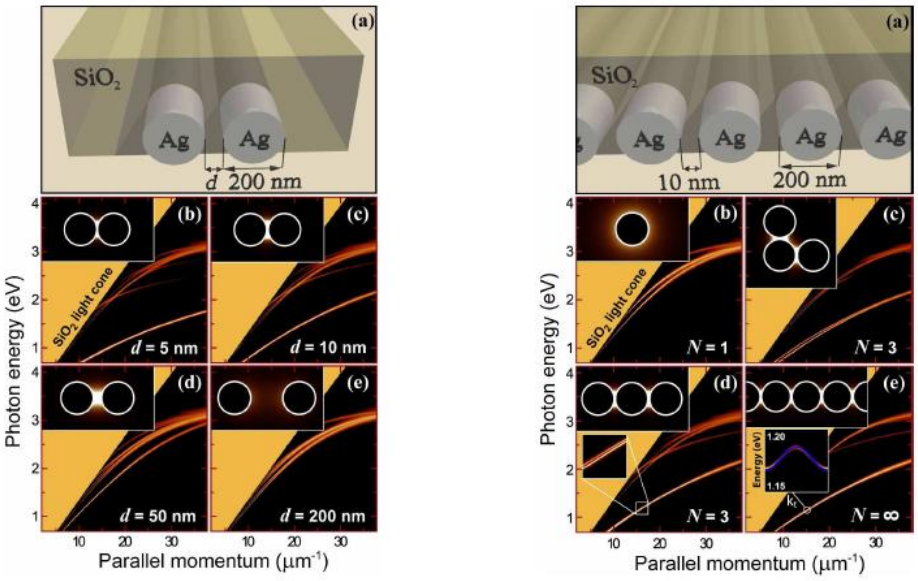

Figure 2.2: A.Manjavacas and F.J.Garcia de Abajo arXiv:0806.1881v1

within the plasmon waveguide structure.In the experiment, the decay length is around $50\mu m$, while theoretical simulations predict a decay length in the order of $500\mu m$.

Manjavacas and Garcia de Abajo [16] recently demonstrated further possibility for plasmonic circuits. They used square and circular sivler nanowire array in silica to form a versatile and tunable platform for highly-integrated plasmon interconnects (Fig 2.2). In this plasmon guided modes, the photon propagation distance and degree of confinement depend strongly on the separation distance between wires. At large separation, one observes only the individual mode. As soon as the spacing is reduced, mode hybridization is reduced. Gap modes occur at small separations, highly localized in the regions between two adjacent wires. In Figure2.2, the gap plasmon modes of two parallel silver nanowires is shown on the left side. (a) is the schematic view of the geometry. $(b) - (e)$ show the photonic density of state as the function of energy and momentum, parallel to the wires for various dimer separations d. The insets show the spatial distribution of the local density of states for the lowest energy gap mode at a free-space light wavelength of $1550nm$. On the right side of Figure2.2 is the evolution of gap plasmon modes with the nanowire number in the array. In (a) is again the schematic

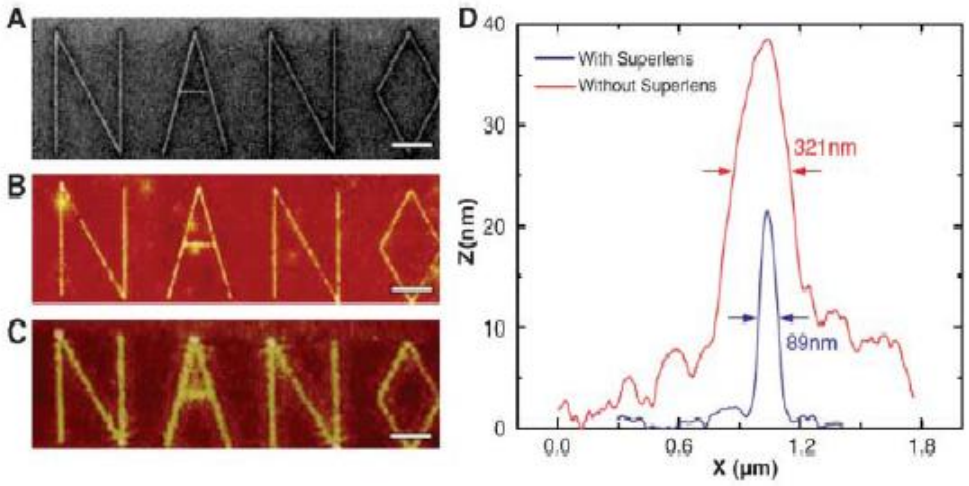

Figure 2.3: N.Fang,H.Lee,C.Sun,X.Zheng, Science 308,534(2005)

view of the geometry. $(b)-(c)$ is the DOS as the function of energy and momentum parallel to the wires for arrays of $N = 1, 3\, and\, \infty$ nanowires. The insets show LDOS maps for the lowest-frequency gap mode at a wavelength of 1550 nm.

These gap modes we have seen, are quite robust against unintended variations of wire cross section or curvature. Furthermore, the gap modes are highly confined to the gap region, so that intermixing between neighboring wire-dimers can be minimized. This scheme is probably the solution for highly-integrated plasmonic circuits in three dimensional spaces.

2.2 Plasmonic Nanolithography

The performance of nanolithography can be admirable improved by Plasmonic.
Pendry[17, 18] introduced the concept "superlens". A superlens can be used to enhance evanescent wave by the excitation of surface plasmons. The gain obtained from plasmonic excitation inside the superlens compensates for the loss of the evanescent waves outside of the superlens. The reconstructed evanescent waves can then be used to restore an image below the diffraction limit on the other side of the lens. The lens is made of a thin slab of material

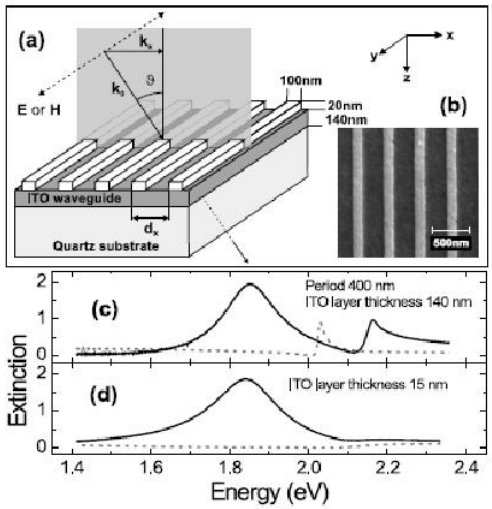

Figure 2.4: A.Christ, H.Giessen et al. Phys.Rev.Lett 91 18391,2003

with negative permittivity and permeability. In Fig2.3A, the word "NANO" was printed as a mask by a focused ion beam system(FIB). Figure 2.3B was obtained with the superlens, the resulting image is almost perfect. Fig2.3C is the diffraction limited image obtained from the conventional lithography. Fig2.3D compares both methods: the plasmonic nanolithography method was able to generate image of much better resolution.

2.3 Waveguide-Plasmon Polaritons

The coupling between localized particle plasmons and optical waveguide modes leads to strong modifications of the transmission light in metallic nanowire arrays on dielectric waveguide substrates. Experiments (A.Christ et al) show evidence for the formation of a new quasiparticle, or waveguide-plasmon polariton[19]. They investigated one-dimensional periodic gold nanowire arrays on top of a dielectric waveguide system. The extinction spectra showed peaks with a complex behavior against period and angle, where the maxima correspond to the resonant modes. In Figure2.4C, the narrow peaks (dash line) in the TE spectra are there due to excitation of TE quasiguided modes. They are example of Fano-type resonances caused by the interaction of the discrete waveguide mode with photon continuum.

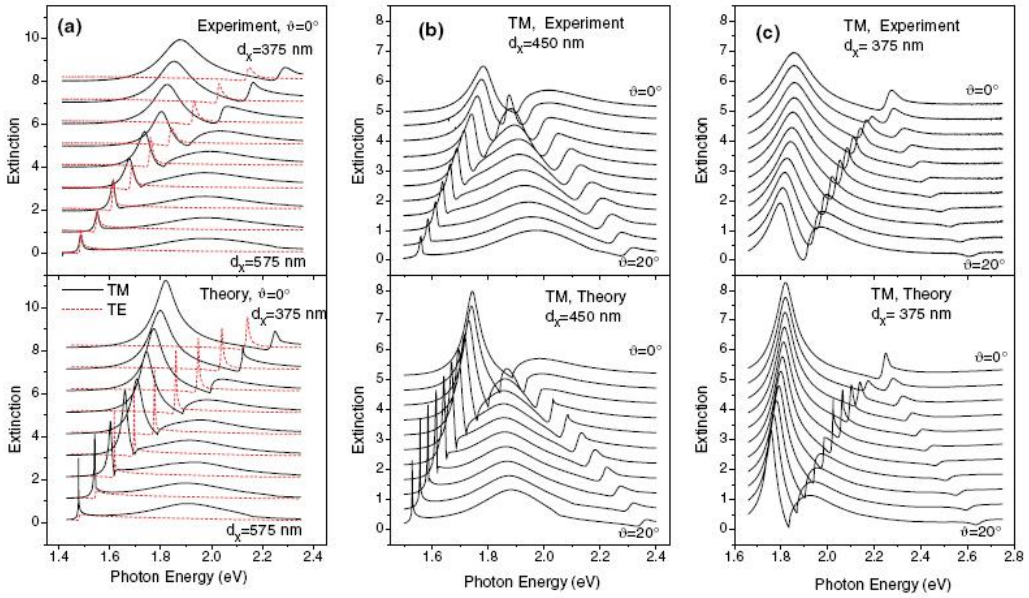

Figure 2.5: Extinction Spetra adapted from [19]

In the TM polarization (solid lines in Fig2.4 and 2.5), there are one broad peak and other narrow peaks. The broad peak is due to the particle plasmon in individual gold wire. If the period or angle is changed, the broad plasmon line shows an anticrossing behavior with the narrower TM-waveguide resonances(Fig 2.5). The anticrossing behavior can be explained by considering a new quasiparticle, the polaritons. On the other hand, one can say the anticrossing behavior are evidence for the existence of polariton quasiparticles.

According to the results, two polariton mode are observed (see Fig2.6). The splitting between the lower and upper polariton mode branches is about $250meV$. We notice that the lower polariton mode is mainly due to the plasmon in goldwire, which is not depend on the period of the goldwire. In contrast, the upper polariton mode is considerably influenced by the period.

Sofar we have present several experiments. In fact, they are all related to photon-electron coupling. Thus is in our interest to study photon-electron coupling theoretically. Photons in the laser beam have non-thermal distribution function. They are out of equilibrium. We will need Keldysh Green's function formalism to calculate this nonequilibrium problem. Next chapter we will introduce Keldysh Green's function formalism.

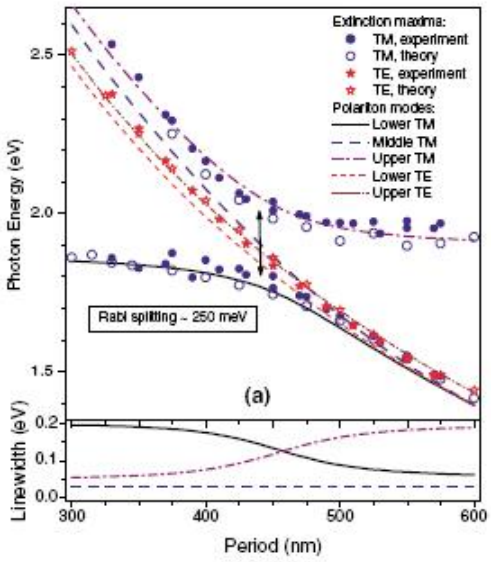

Figure 2.6: Polariton mode adapted from [19]

Chapter 3

Plasmon Antiresonance and particle-hole excitation with external field

3.1 Plasmon-Fano Resonance

Exchange and correlation effects in the excitation spectra of nearly-free-electron systems, such as metals and sp-band semiconductors have been of great research interests [20, 21, 22, 23]. It has been shown that local-field effects in simple metals and semiconductors couple the plasmon into the particle-hole excitation spectrum, leading to a plasmon antiresonance (Plasmon-Fano Resonance) [24]. External light interacting with periodically nanostructured metal sufaces has also been intensive studied [25, 26, 27], even to three-dimensional [28]. Extraordinary transmission with resonant phenomena has been observed in subwavelength hole arrays [29]-[36], metallic grating [37]-[40]. absorption of the incoming radiation[41]-[45], and coherent thermal emission[46]-[48].

Plasmon-Fano Resonance has even observed in carbon nanotubes[49], which have been of great interests in chemistry, physics, electronics, and material science [50, 51], and have the potential for future nanoengineering [52, 53].

The mathematic form of fano resonance is

$$\frac{(q+\epsilon)^2}{(1+\epsilon^2)} = 1 + \frac{q^2 + 2q\epsilon - 1}{(1+\epsilon^2)} \qquad \epsilon = \frac{E - E_0}{\Gamma/2} \tag{3.1}$$

where q is the Fano-Parameter. In Feshbach?Fano partitioning theory it is interpreted as the ratio between the resonant and direct scattering probability. Γ is the line width, E_0 is the position of the resonance. ϵ is the reduced energy.

3.1.1 Plasmon Resonance in Photonic Crystals

Plasmonic and photonic resonances by metallic photonic crystals have been the subject of intensive studies [54]-[61]. A lot of research activities take advantage of template-assisted assembly of micorporous and nanoporous metal sturcture to produce periodically arranged nanopores[62, 63]. Extraordinary transmission and absorption of light caused by excitation of plasmons in nanopores have been theoretically predicted[65, 66], and observed by experiment [62]. These knowledge help to tune the optical properties of metallic photonic crystals by nano-engineering the structure parameters.

3.1.2 Plasmon mode coupling

Optical properties of metal surfaces can be influenced by the coulping of different plasmon modes. The surface plasom excitation, so called plasompolaritons, are usually propagating on the metal planar surface. Systems with delocalized surface plasom have optical properties different to those with delocalized plasmon. It is quantitatively and experimentally demonstrated, the coupling of two or more plasom mode leads to spetral shift and other optical property variation [68, 69].

3.1.3 Plasmon Coupled to External Environment

The radiative coupling between surface plasmon and its electromagnetic environment arises fundamental quantum-optical phenomena like vaccum Rabi or normal mode splitting [70]-[73]. Radiative coupling have been studied for various quantum system, for example, single atoms [70], semiconductor quantum dots [72], quantum wells coupled to microcavity [73, 74]. The coherent coupling between surface plasmon polaritons and excitons in a hybrid metal-semiconductor nanostructures has also been observed [75]. Metallic nanostructures

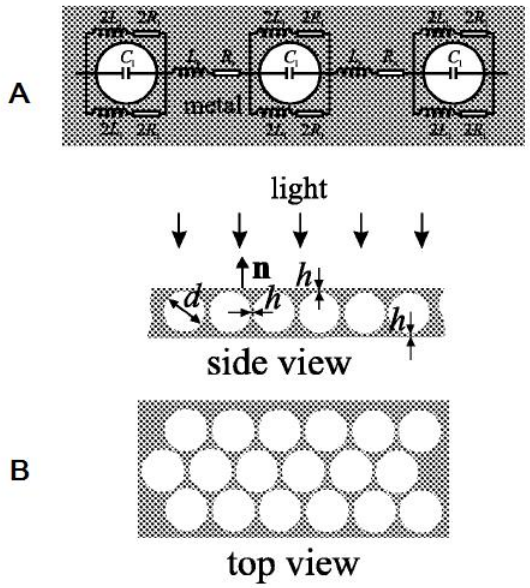

Figure 3.1: A Equivalent ciruit to the Lattice of voids; B the lattice of voids

3.2 Simple Model for optical plasmonic properties of planar surface

The essential physics of optical properties of a 2D lattice of voids in metal (see Fig3.1 B) are described by the equivalent impedance Z_{eff}. From the Drude model, the conductivity of the metal is

$$\sigma_e(\omega) = \frac{e^2 N_e}{m(\nu_e - i\omega)} \tag{3.2}$$

whhere e and m are the electron charge and mass, N_e is the bulk free electron density, ν_e is the free electron scattering rate. The effective areal impedance can be written as

$$Z_e = \frac{1}{\sigma_e \delta} = R_e - i\omega L_e \tag{3.3}$$

where δ is the metal characteristic skin depth. The effective areal electronic resistance $R_e = m\nu_e/(e^2\delta N_e)$ determines the amount of power absorbed, and the areal reactance $-\omega L_e$ concerns the phase shift of the electric field.

An equivalent RLC circuit (see Fig 3.1 A) was suggestted in [66] to describe the plasma oscillations. The Effective areal impedance to the lth mode is related to RLC circuit by

$$Z_l = \frac{R_l - i\omega L_l}{1 - \omega^2 L_l C_l - i\omega R_l C_l} \tag{3.4}$$

with phenomenological assumptions $R_l = 2m\nu_l/(e^2\Delta_l\delta N_e)$, $L_l = m/(e^2\Delta_l\delta N_e)$, and $C_l = |f_l|^2 d\epsilon_0$, one finds

$$Z_l = \frac{m}{e^2\Delta_l\delta N_e}\frac{\omega_l^2(2\nu_l - i\omega)}{\omega_l^2 - \omega^2 - 2i\omega\nu_l} \tag{3.5}$$

where

$$\omega_l = \sqrt{\frac{e^2\Delta_l\delta N_e}{|f|^2 d\epsilon_0 m}} \tag{3.6}$$

ν_l is the damping of the lth plasmon mode, Δ_l is the fraction of free electrons participating in the plasma osillations at lth mode, d is the void diameter, ϵ_0 is the electrical constant, $|f_l|^2$ is the dimensionless factor. At the vicinity of the resonance $\omega \simeq \omega_l$, assuming $\nu_l \ll \omega_l$, the total effective areal impedance is

$$Z_{eff} \simeq -i\frac{m|\beta_l|^2}{2e^2\Delta_l\delta N_e}\frac{\omega_l^2}{\omega_l - \omega - i\nu_l} \tag{3.7}$$

$|\beta_l|^2$ is the phenomenological coefficient of coupling between the external oscillating electric field and the lth plasmon mode.

3.3 The Hubbard Model With A Driving External Field

The coupling of plasmon to external field is already investigated in the Hubbard model for hypercubic lattice in the limit of infinite dimensions [67].

The Hamiltonian is

$$H = -\sum_{<ij>\sigma} t_{ij}(c_{i\sigma}^\dagger c_{j\sigma} + c_{j\sigma}^\dagger c_{i\sigma}) + U\sum_i n_{i\uparrow}n_{i\downarrow} + \sum_{i\sigma} V_i(t)c_{i\sigma}^\dagger c_{i\sigma} \tag{3.8}$$

where $c^\dagger(c)$ is the fermion creation(annihilation) operator, U is the coulomb interaction constant. The third term describes an external time-dependent field with frequency Ω and wave vector q.

$$V_i(t) = Acos(\Omega t - qx_i) \tag{3.9}$$

In momentum space representation, the coupling term can be written as

$$\sum_{i\sigma} V_i(t) c^\dagger_{i\sigma} c_{i\sigma} = \sum_{k\sigma} \frac{A}{2} (c^\dagger_{k+q\sigma} c_{k\sigma} e^{-i\Omega t} + c^\dagger_{k-q\sigma} c_{k\sigma} e^{i\Omega t}) \tag{3.10}$$

3.4 Outlook for Further Theoretical Model

The model above treats the external field in classical description, $V_i(t) = Acos(\Omega t - qx_i)$. We will quantize the photon field, introduce Green's function to describe photons. The external field is nonhomogenous and nonequilibrium. Therefore we need to apply nonequilibrium Green's function, also known as Keldysh Green's function formalism. The next chapter gives an introduction to Keldysh Green's function formalism.

Chapter 4

Kelysh Green's Function Formalism

4.1 Introduction

The schrodinger equation is one of the basis to the quantum theory.[76]:

$$i\frac{\partial}{\partial t}\Psi(r_1, r_2, ..., r_N, t) = \mathscr{H}\Psi(r_1, r_2, ..., r_N, t) \tag{4.1}$$

This equation is only solvable at very simple situation like single particle inside one dimensional rectangle potential trap. For more than 2 body physical system, it would be not easy to obtain a analytical solution for the Schrodinger's equation. Our world is always complex, full of diversity and variety, so solving the Schrodinger equation exatly is not possible, far beyond the ability of the computing power. One of the ideas to solve them is to use Green's function.

Green's Functions are propagators representing the particles[77]. Once the Green's functions are calculated, many property of the system can also be calculated. Green's functions are among the most methods in condensed matter physics.

There are kinds of many-particle Green's function for specific purpose. In equilibrium theory, there are zero-temperature and finite temperature formalism.[78, 79, 80]

We are going to use a more general nonequilibrium Green's Function formalism, first introduced by P.C.Martin[81] and J.Schwinger[82] and

L.V.Keldysh[83]. Further Development was done by Kadanoff and Baym[84]. A detailed review of this method is given by J.Rammer and H.Smith[85].

4.2 Various Quantum Mechanical Pictures

The Keldysh method is based on real-time Green's functions. It is designed to handle physical systems with explicitely time-dependent Hamiltonian

$$H = H_0 + H^i \tag{4.2}$$

where H_0 is the non-interacting Hamiltonian. Only with this non-interacting Hamiltonian, it is usually a strictly solvable problem. The H^i is the Hamiltonian describing the interactions among particles, for example the coulomb interaction.

We consider a general system, which is in contact with a heat bath of temperature T and a particle reservoir whose chemical potential is μ. Considering a grand canonical ensemble, the state of system in thermodynamic equilibrium is described by the equilibrium density operator:

$$\rho(H) = \frac{e^{-\beta H}}{T_r[e^{-\beta H}]} \tag{4.3}$$

$T_r[]$ denotes the trace of the matrix. We have chosen $\mu = 0$, that means we are going to measure the particle energy with respect to $\mu = 0$. In order to understand the non-equilibrium problem, we assume that the system is in thermodynamic equilibrium until the time t_0. And then the system is instantaneously disconnnected from the reservoirs, then a disturbance comes to the system, who gives rise to a non-equilibrium situation. This disturbance can be many things like time varying electric-magnetic field or laser pulse. We denote this disturbance $H_d(t)$. Than we can write our total time-dependent hamiltonian $\mathscr{H}$ as

$$\mathscr{H} = H + H_d(t) \tag{4.4}$$

$$H_d(t) = 0, \quad t < t_0 \tag{4.5}$$

H is defined in Eq.(3.2). Now we want to calculate the nonequilibrium expectation values of operators corresponding to physical observables. In Heisenberg picture, the state vectors are time independent. On the other hand, the

operators are time dependent. We are going to write the expection value of observable in Heisenberg picture.

$$< O_{\mathscr{H}(t)} >= T_r[\rho(H)O_{\mathscr{H}(t)}] \tag{4.6}$$

where the $O_{\mathscr{H}(t)}$ is the observable in the Heisenberg picture. It is important to notice the $H_d(t)$ is not included in the density operator ρ. It is discussed by Mahan[79]. One should not include $H_d(t)$ directly in ρ. In order to understand the description of the non-equilibrium problem, it is important to understand various quantum mechanical pictures. We shall start with the Schrodinger equation:

$$i\hbar\partial_t|\Psi_S(t)\rangle = \mathscr{H}(t)|\Psi_S(t)\rangle \tag{4.7}$$

The ket $|\Psi_S(t)\rangle$ is the abstract state vector in Schrodinger picture. We can integrate Eqa(3.7)

$$|\Psi_S(t)\rangle - |\Psi_S(t_0)\rangle = -i\hbar^{-1}\int_{t_0}^{t} dt_1 \mathscr{H}(t_1)|\Psi_S(t_1)\rangle \tag{4.8}$$

If one does it iterately,

$$\begin{aligned}|\Psi_S(t)\rangle = \sum_{n=0}^{\infty}\frac{(-i\hbar^{-1})^n}{n!}\int_{t_0}^{t} dt_1\int_{t_0}^{t_1} dt_2\cdots\int_{t_0}^{t_{n-1}} dt_n \\ \mathscr{H}(t_1)\mathscr{H}(t_2)\ldots\mathscr{H}(t_n)|\Psi_S(t_0)\rangle\end{aligned} \tag{4.9}$$

The above equation can be written as a shorter form

$$|\Psi_S(t)\rangle = \sum_{n=0}^{\infty}\frac{(-i\hbar^{-1})^n}{n!}\int_{t_0}^{t} dt_1\cdots\int_{t_0}^{t_{n-1}} dt_n \mathcal{T}_t\{\mathscr{H}(t_1)\ldots\mathscr{H}(t_n)\}|\Psi_S(t_0)\rangle \tag{4.10}$$

The $\mathcal{T}_t$ is the usual time-ordering operator that organizes all the other operators behind him by their time arguments.

$$\begin{aligned}\mathcal{T}_t\{O_1(t_1)O_2(t_2)\ldots O_n(t_n)\} = (\pm)^P O_{i_1}(t_{i_1})O_{i_2}(t_{i_2})\ldots O_{i_n}(t_{i_n}) \\ t_{i_1} > t_{i_2} > \cdots > t_{i_n}\end{aligned} \tag{4.11}$$

O_{i_n} are either fermion operators or boson operators. In $(\pm)^P$, plus sign is for bosons and minus sign for fermions. P is the number of interchanges of

operators from their original given order. For a Hamiltonian containing an even number of fermion fields this sign is always positive.
If we want to use the Heisenberg picture, the operators are no longer time-independent. Instead, the state vectors are time-independent. The following equation relates the two pictures.

$$\langle \Psi_S(t)|O_S|\Psi_S(t)\rangle = \langle \Psi_{\mathscr{H}}|O_{\mathscr{H}}(t)|\Psi_{\mathscr{H}}\rangle \tag{4.12}$$

$|\Psi_S(t)\rangle$ stands for state in Schrodinger picture, and $|\Psi_{\mathscr{H}}\rangle$ stands for state in Heisenberg picture. If we choose the pictures to coincide at time t_0 ,then $|\Psi_{\mathscr{H}}\rangle = |\Psi_S(t_0)\rangle$ The operators from the two different pictures have the relation

$$O_{\mathscr{H}}(t) = u^{\dagger}_{\mathscr{H}}(t,t_0)O_S u_{\mathscr{H}}(t,t_0) \tag{4.13}$$

$u_{\mathscr{H}}(t,t_0)$ is called evolution operator with respect to $\mathscr{H}$.From Eq.(3.10) we see

$$\begin{aligned} u_{\mathscr{H}}(t,t_0) &= \sum_{n=0}^{\infty} \frac{(-i\hbar^{-1})^n}{n!} \int_{t_0}^{t} dt_1 \cdots \int_{t_0}^{t_{n-1}} dt_n \mathcal{T}_t\{\mathscr{H}(t_1)\ldots\mathscr{H}(t_n)\} \\ &= \mathcal{T}_t\{e^{-i\hbar^{-1}\int_{t_0}^{t} dt' \mathscr{H}(t')}\} \end{aligned} \tag{4.14}$$

We have expressed the Operator $O_{\mathscr{H}}(t)$ in Heisenberg picture. Now we try to find out the operator with a evolution operator, which is governed by the time-independent part H

$$O_H(t) = u^{\dagger}_H(t,t_0)O_S u_H(t,t_0) \tag{4.15}$$

now the time evolution operator with respect to H is given by

$$u_H(t,t_0) = e^{-i\hbar^{-1}H(t-t_0)} \tag{4.16}$$

There is relation between $O_{\mathscr{H}}$ and O_H

$$O_{\mathscr{H}}(t) = u^{\dagger}_{\mathscr{H}}(t,t_0)u_H(t,t_0)O_H u^{\dagger}_H(t,t_0)u_{\mathscr{H}}(t,t_0) \tag{4.17}$$

We define

$$v_H(t,t_0) = u^{\dagger}_H(t,t_0)u_{\mathscr{H}}(t,t_0) \tag{4.18}$$

Then we can write

$$O_{\mathscr{H}}(t) = v^{\dagger}_H(t,t_0)O_H(t,t_0)v_H(t,t_0) \tag{4.19}$$

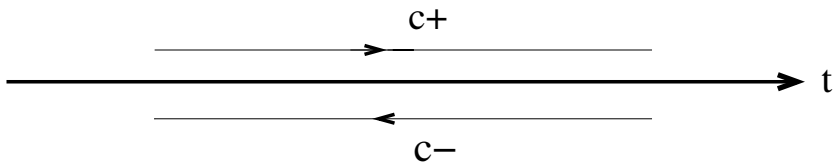

Figure 4.1: The Keldysh Contour

Differentiating $v_H()$ with respect to t

$$\begin{aligned} i\hbar\partial_t v_H(t,t_0) &= [i\hbar\partial_t u_H^\dagger(t,t_0)]u_{\mathscr{H}}(t,t_0) + u_H^\dagger(t,t_0)[i\hbar\partial_t u_{\mathscr{H}}(t,t_0)] \\ &= [-Hu_H^\dagger(t,t_0)] + u_H^\dagger(t,t_0)[\mathscr{H}(t)u_{\mathscr{H}}(t,t_0)] \\ &= -Hv_H^\dagger(t,t_0) + u_H^\dagger(t,t_0)\mathscr{H}(t)u_H(t,t_0)u_H^\dagger(t,t_0)u_{\mathscr{H}}(t,t_0) \\ &= -Hv_H^\dagger(t,t_0) + \mathscr{H}(t)v_H(t,t_0) \\ &= H_d(t)v_H(t,t_0) \end{aligned} \tag{4.20}$$

if one integrates the above equation, similar to Eq(3.15),one finds

$$v_H(t,t_0) = \mathcal{T}_t\{e^{-i\hbar^{-1}\int_{t_0}^{t} dt' H_d(t')}\} \tag{4.21}$$

The ordinary time-ordering can also be written as the contour ordering as depicted in [Fig4.1]. This contour consists of two parts, c_+ and c_-. t_1 on c_+ is always ealier than a time t_2 on c_-. Thus we can write

$$v_H(t,t_0) = \mathcal{T}_{c_+}\{e^{-i\hbar^{-1}\int_{c_+} d\tau H_d(\tau)}\} \tag{4.22}$$

$$v_H^\dagger(t,t_0) = \mathcal{T}_{c_-}\{e^{-i\hbar^{-1}\int_{c_-} d\tau H_d(\tau)}\} \tag{4.23}$$

$\mathcal{T}_c$ is the contour-ordering operator that organizes a product of operators according to the sequence of their time arguments on the contour depicted in Fig4.1.
Thus the operator in Eq.(3.19) can be written as

$$O_{\mathscr{H}}(t) = \mathcal{T}_{c_-}\{e^{-i\hbar^{-1}\int_{c_-} d\tau H_d(\tau)}\}O_H(t)\mathcal{T}_{c_+}\{e^{-i\hbar^{-1}\int_{c_+} d\tau H_d(\tau)}\} \tag{4.24}$$

Combine the two contours. $c = c_+ + c_-$, write it in a compact form

$$O_{\mathscr{H}}(t) = \mathcal{T}_c\{e^{-i\hbar^{-1}\int_c d\tau H_d(\tau)}\}O_H(t) \tag{4.25}$$

With Eq(3.26), we have an expression, where the nonequilibrium disturbance part $H_d(t)$ is separated from the other part of the Hamiltonian, and the time-evolution of the operators are governed by H only.

4.2.1 The Interaction Picture

Remember $H = H_0 + H^i$, now we want a simpler situation where the time evolution operator is only governed by H_0. The interaction picture is defined by

$$O_{H_0}(t) = u^\dagger_{H_0}(t,t_0) O_S u_{H_0}(t,t_0) \tag{4.26}$$

The evolution operator is given by

$$u_{H_0}(t,t_0) = e^{-i\hbar^{-1}H_0(t-t_0)} \tag{4.27}$$

Similar to the derivation in Heisenberg picture, we have

$$O_{\mathscr{H}}(t) = u^\dagger_{\mathscr{H}}(t,t_0) u_{H_0}(t,t_0) O_H u^\dagger_{H_0}(t,t_0) u_{\mathscr{H}}(t,t_0) \tag{4.28}$$

with further definiton

$$v_{H_0}(t,t_0) = u^\dagger_{H_0}(t,t_0) u_{\mathscr{H}}(t,t_0) \tag{4.29}$$

Then we can write

$$O_{\mathscr{H}}(t) = v^\dagger_{H_0}(t,t_0) O_{H_0}(t,t_0) v_{H_0}(t,t_0) \tag{4.30}$$

Differentiating $v_{H_0}()$ with respect to t

$$\begin{aligned} i\hbar\partial_t v_{H_0}(t,t_0) &= [i\hbar\partial_t u^\dagger_{H_0}(t,t_0)] u_{\mathscr{H}}(t,t_0) + u^\dagger_{H_0}(t,t_0)[i\hbar\partial_t u_{\mathscr{H}}(t,t_0)] \\ &= [-H_0 u^\dagger_{H_0}(t,t_0)] + u^\dagger_{H_0}(t,t_0)[\mathscr{H}(t) u_{\mathscr{H}}(t,t_0)] \\ &= -H_0 v^\dagger_{H_0}(t,t_0) + u^\dagger_{H_0}(t,t_0)\mathscr{H}(t) u_{H_0}(t,t_0) u^\dagger_{H_0}(t,t_0) u_{\mathscr{H}}(t,t_0) \\ &= -H_0 v^\dagger_H(t,t_0) + \mathscr{H}(t) v_H(t,t_0) \\ &= \{H^i + H_d(t)\} v_{H_0}(t,t_0) \end{aligned} \tag{4.31}$$

Similarly, we have the expression for v_{H_0}

$$v_{H_0}(t,t_0) = \mathcal{T}_t\{e^{-i\hbar^{-1}\int_{t_0}^t dt'(H^i + H_d(t'))}\} \tag{4.32}$$

Then we see, the relation between the interaction picture and Heisenberg picture is

$$\begin{aligned} O_{\mathscr{H}}(t) &= \mathcal{T}_c\{e^{-i\hbar^{-1}\int_c d\tau H_d(\tau)} e^{-i\hbar^{-1}\int_c d\tau H^i(\tau)} O_{H_0}(t)\} \\ &= \mathcal{T}_c\{S^d_c S^i_c O_{H_0}(t)\} \end{aligned} \tag{4.33}$$

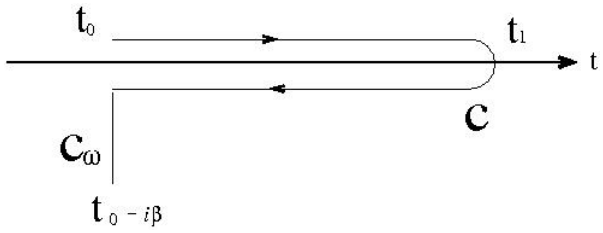

Figure 4.2: The contour $\bar{c} = c \cup c_\omega$ are used in the transformation into the interaction picture of H_0

with

$$S_c^d = e^{-i\hbar^{-1}\int_c d\tau H_d(\tau)} \tag{4.34}$$

$$S_c^i = e^{-i\hbar^{-1}\int_c d\tau H^i(\tau)} \tag{4.35}$$

The next step is to write the quantum mechanical average of the O_{H_0} in the interaction picture. First of all, we need to replace the ensemble average with respect to $\rho(H)$ by $\rho(H_0)$. For the convenience,we define a operator $k(t,t_0)$

$$k(t,t_0) = \mathcal{T}_t\{v_{H_0}^\dagger(t,t_0)v_H(t,t_0)\} \tag{4.36}$$

Differentiating $k(t,t_0)$ with respect to t

$$\begin{aligned} i\hbar\partial_t k(t,t_0) &= -[H^i(t) + H_d(t)]k(t,t_0) + H_d(t)k(t,t_0) \\ &= -H_d(t)k(t,t_0) \end{aligned} \tag{4.37}$$

The solution of $k(t,t_0)$ comes out to be

$$k(t,t_0) = \mathcal{T}_t\{e^{-i\hbar^{-1}\int_{t_0}^t dt' H_d(t')}\} \tag{4.38}$$

Comparing $k(t,t_0)$,$u_H(t,t_0)$ and $u_{H_0}(t,t_0)$ we find out that

$$u_H(t,t_0) = u_{H_0}(t,t_0)k(t,t_0) \tag{4.39}$$

remembering that $u_H(t,t_0) = e^{-i\hbar^{-1}H(t-t_0)}$ and $u_{H_0}(t,t_0) = e^{-i\hbar^{-1}H_0(t-t_0)}$,we see

$$e^{\beta H} = e^{\beta H_0}k(t_0 - i\beta, t_0) \tag{4.40}$$

We are now able to write the ensemble average

$$\begin{aligned} \langle O_{\mathscr{H}}(t)\rangle &= \frac{T_r[e^{-\beta H}O_{\mathscr{H}}(t)]}{T_r[e^{-\beta H}]} \\ &= \frac{T_r[e^{-\beta H_0}k(t_0 - i\beta, t_0)O_{\mathscr{H}}(t)]}{T_r[e^{-\beta H_0}k(t_0 - i\beta, t_0)]} \end{aligned} \tag{4.41}$$

Now we are going to use a notation $\langle \dots \rangle_0$, which denote the ensemble average with respect to $\rho(H_0)$, then the ensemble average can be written as

$$\langle O_{\mathscr{H}}(t)\rangle = \frac{\langle k(t_0 - i\beta, t_0) O_{\mathscr{H}}(t)\rangle_0}{\langle k(t_0 - i\beta, t_0)\rangle_0} \tag{4.42}$$

The operator $k(t_0 - i\beta, t_0)$ defines a contour section c_β, which runs along a imaginary time axis from $t = t_0$ to $t = t_0 - i\beta$. Besides, one has to notice the fact that

$$\mathcal{T}_c\{e^{-i\hbar^{-1}\int_c d\tau H_d(\tau)} e^{-i\hbar^{-1}\int_c d\tau H^i(\tau)}\} = 1 \tag{4.43}$$

We combine this imaginary time course with the original one, we call this new contour $\bar{c}$

$$\bar{c} = \ c \cup c_\omega \tag{4.44}$$

then $k(t_0, t_0 - i\beta)$ can be written as

$$\begin{aligned} k(t, t_0) &= \mathcal{T}_{\bar{c}}\{e^{-i\hbar^{-1}\int_c d\tau H_d(\tau)}\ e^{-i\hbar^{-1}\int_{\bar{c}} d\tau H^i(\tau)}\} \\ &= \mathcal{T}_{\bar{c}}\{S_c^d S_{\bar{c}}^i\} \end{aligned} \tag{4.45}$$

with

$$S_c^d = e^{-i\hbar^{-1}\int_c d\tau H_d(\tau)} \tag{4.46}$$

$$S_{\bar{c}}^i = e^{-i\hbar^{-1}\int_{\bar{c}} d\tau H^i(\tau)} \tag{4.47}$$

At last, we can write the ensemble average as

$$\langle O_{\mathscr{H}}(t)\rangle = \frac{\langle \mathcal{T}_{\bar{c}}\{S_c^d S_{\bar{c}}^i O_{H_0}\}\rangle_0}{\langle \mathcal{T}_{\bar{c}}\{S_c^d S_{\bar{c}}^i\}\rangle_0} \tag{4.48}$$

The advantage of this ensemble is that we separate the H^i and H_d from the density matrix ρ. The ensemble matrix is now to evaluate with the non-interacting density matrix $\rho(H_0)$. In other words, all the time dependence of the ensemble is decided by the simple part H_0, which is exactly solvable. The difficult parts are handled in S_c^d and $S_{\bar{c}}^i$, where one can do perturbation expansion.

In the most situations, we focus in steady state problem. We simply let $t_0 \to \ -\infty$. It means the non-equilibrium disturbance is considered to be turned on for a suffient time, so suffient that the system becomes steady. If the interactions among the particles are turned on adiabatically, we have:

$$\lim_{t_0 \to -\infty} k(t_0 - i\beta, t_0) = \lim_{t_0 \to -\infty} \mathcal{T}_{\bar{c}}\{e^{-i\hbar^{-1}\int_{t_0}^{t_0 - i\beta} dt H^i(t)}\} = 1 \tag{4.49}$$

4.3 Green's Functions

As mentioned at the beginning of this introduction, we need to calculate the Green's functions. Green's functions are powerful in many particle physics because they contain much information about the system. In non-equilibrium system, instead of time order Green's functions, we are going to evaluate the contour-ordering single particle Green's function

$$G^c(i,j) = -i\hbar^{-1}\langle \mathcal{T}_c\{\Psi_{\mathscr{H}}(i)\Psi^\dagger_{\mathscr{H}}(j)\}\rangle \tag{4.50}$$

where $\Psi_{\mathscr{H}}$ is the field operator in the Heisenberg picture. The argument stands for a short-hand notation

$$i = (r_i, \sigma, t_i) \tag{4.51}$$

The field operators are linear combinations of the creation and annihilation operators

$$\Psi(r,\sigma) = \sum_k \psi_k(r) c_{k\sigma} \tag{4.52}$$

and

$$\Psi^\dagger(r,\sigma) = \sum_k \psi^*_k(r) c^\dagger_{k\sigma} \tag{4.53}$$

$\psi_k(r)$ and $\psi^*_k(r)$ are the single particle wave functions. $c_{k\sigma}$ and $c^\dagger_{k\sigma}$ are the annihilation and creation operator. They raise or lower the occupation of particles in the state $|k\sigma\rangle$. The sum is over a complete set of quantum numbers.

The nonequilibrium steady state Green's function can be written in the interaction picture that is discussed in the previous section.

$$G^c(i,j) = -i\hbar^{-1}\frac{\langle \mathcal{T}_c\{S^d_c S^i_c \Psi_{H_0}(i)\Psi^\dagger_{H_0}(j)\}\rangle_0}{\langle \mathcal{T}_c\{S^d_c S^i_c\}\rangle_0} \tag{4.54}$$

With this expression, one can easily see the way to do perturbation theory. The numerator and denominator are ready to be expand.Then one can apply Wick's theorem similarly as one had done in the equilibrium theory with normal time-ordering Green's function. They are discussed in many standard many-body physics textbooks. They have given knowledge the Wick's theorem and Feynman rules and diagram representations. Theses are also valid in

non-equilibrium theory, because the denominator exactly cancels the disconnected diagrams. In the perturbation theory, one calculates the connected diagram from different order expansion of S_c^d and S_c^i.

The perturbation expansion in nonequilibrium theory with contour-ordered single particle Green's function $G(i,j)$ is similar to the time-ordered single-particle Green's function in equilibrium theory. The only difference is the time integrations over the real axis are replaced by contour integrations along c.

The contour-ordered Green's function G^c can be mapped into the Keldysh space[79]

$$G^c \longrightarrow \hat{G} = \begin{bmatrix} G^{++} & G^{+-} \\ G^{-+} & G^{--} \end{bmatrix} \tag{4.55}$$

where $\pm$ specifies which time argument lies on the upper (+) contour and which lies on the lower time contour. G^{++} is the usual time-ordered Green's function and G^{--} is the anti-time-ordered Green's function. The remaining two components are correlation functions

$$G^{++}(i,j) = -i\langle \mathcal{T}[\psi(i)\psi^\dagger(j)]\rangle \tag{4.56}$$

$$G^{--}(i,j) = -i\langle \tilde{\mathcal{T}}[\psi(i)\psi^\dagger(j)]\rangle \tag{4.57}$$

$$G^{+-}(i,j) = \pm i\langle \psi^\dagger(j)\psi(i)\rangle \tag{4.58}$$

$$G^{-+}(i,j) = -i\langle \psi(i)\psi^\dagger(j)\rangle \tag{4.59}$$

In the equation for G^{+-}, the upper sign is for fermion,and the lower sign is for boson.

The anti-time-ordering operator $\tilde{\mathcal{T}}$ is defined as

$$\tilde{\mathcal{T}}[\psi(i)\psi^\dagger(j)] = \begin{cases} \psi(i)\psi^\dagger(j) & \text{if } t_i \le t_j \\ \mp\psi^\dagger(j)\psi(i) & \text{if } t_i > t_j \end{cases} \tag{4.60}$$

The components of the Keldysh matrix are not independent. From the definitions we know that they are related linearly

$$G^{++} + G^{--} = G^{+-} + G^{-+} \tag{4.61}$$

The functions G^{--} and G^{++} are connected by the relation of "anti-Hermitian conjugacy".

$$G^{++}(i,j) = -G^{--*}(j,i) \tag{4.62}$$

The functions G^{-+} and G^{+-} and themselves anti-Hermitian

$$G^{-+}(i,j) = -G^{-+*}(j,i) \quad G^{+-}(i,j) = -G^{+-*}(j,i) \tag{4.63}$$

It is convenient to calculate the retarded Green's function G^r and advanced Green's function instead of time-ordered G^{++} and anti-time-ordered G^{--}. Because the retarded and advanced Green's functions are directly related to the density of state(DOS) of the particles. The retarded and advanced Green's functions are so defined:

$$G^r(i,j) = -i\hbar^{-1}\theta(t_i - t_j)\langle\psi(i)\psi^\dagger(j) \pm \psi^\dagger(j)\psi(i)\rangle \tag{4.64}$$

$$G^a(i,j) = i\hbar^{-1}\theta(t_j - t_i)\langle\psi(i)\psi^\dagger(j) \pm \psi^\dagger(j)\psi(i)\rangle \tag{4.65}$$

The retarded and advanced Green's function are Hermitian conjugates.

$$G^a(i,j) = G^{r*}(j,i) \tag{4.66}$$

There are more relations between the components.

$$\begin{aligned} G^r &= G^{--} - G^{-+} = G^{+-} - G^{++} \\ G^a &= G^{--} - G^{+-} = G^{-+} - G^{++} \end{aligned} \tag{4.67}$$

if the system is steady and spatial homogeneity, all functions are depending only on the difference $t = t_i - t_j$ and $r = r_i - r_j$. One can do Fourier tranformation to the Green's function. The Fourier components satisfy the equations

$$G^{--}(w,p) = -G^{++*}(w,p) \tag{4.68}$$

$$G^a(w,p) = G^{r*}(w,p) \tag{4.69}$$

Following Eq(3.63) ,the Fourier components $G^{+-}(w,p)$ and $G^{-+}(w,p)$ are purely imaginary.

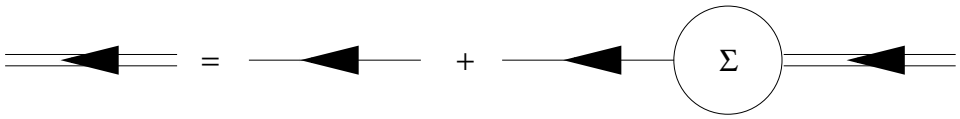

Figure 4.3: Diagrammatic representation of Dyson's equation. The single line is the unperturbed Green's function. The double line is the full Green's function

4.4 Dyson's Equation

with the Dyson's equation we are able to calculate the full Green's function, as long as we know the selfenergy. In the non-equilibrium theory the selfenergy, the same as the Green's functions, is mapped onto the Keldysh space, a matrix with components

$$\hat{\Sigma} = \begin{bmatrix} \Sigma^{++} & \Sigma^{+-} \\ \Sigma^{-+} & \Sigma^{--} \end{bmatrix} \tag{4.70}$$

The contour-ordered single-particle Green's function obeys Dyson's equation. It is a matrix equation in Keldysh space

$$\hat{G}(i,j) = \hat{G}_0(i,j) + \iint dk\ dh\ \hat{G}_0(i,k)\hat{\Sigma}(k,h)\hat{G}(h,j) \tag{4.71}$$

where $\hat{G}_0(i,j)$ is the unperturbed Green's function. A diagrammatic illustration to the Dyson's equation is depicted in Fig4.3. In the Dyson's equation, a short-hand notation has been introduced

$$\int dk = \int dr_k \int dt_k \tag{4.72}$$

We will introduce Langreth's rule and convert the contour integration into real-time integrations.

The set of equations of $\hat{G}$ and $\hat{\Sigma}$ is not directly to be used. It is better to do such a transformation that one of the elements of matrix $\hat{G}$ to be reduced to zero. This can be done by a linear transformation

$$\tilde{G} = R^{-1}\hat{G}R = \begin{bmatrix} 0 & G^a \\ G^r & G^{keld} \end{bmatrix} \tag{4.73}$$

with the transformation matrix

$$R = \frac{1}{\sqrt{2}}\begin{bmatrix} 1 & 1 \\ -1 & 1 \end{bmatrix} \quad R^{-1} = \frac{1}{\sqrt{2}}\begin{bmatrix} 1 & -1 \\ 1 & 1 \end{bmatrix} \tag{4.74}$$

and the Keldysh component is defined by

$$G^{keld} = G^{++} + G^{--} = G^{+-} + G^{-+} \tag{4.75}$$

Due to the Dyson's equation,the matrix $\hat{\Sigma}$ is also transformed by R.

$$\tilde{\Sigma} = R^{-1}\hat{\Sigma}R = \begin{bmatrix} \Sigma^{keld} & \Sigma^{r} \\ \Sigma^{a} & 0 \end{bmatrix} \tag{4.76}$$

with the notation

$$\Sigma^{keld} = \Sigma^{--} + \Sigma^{++} \tag{4.77}$$

$$\Sigma^{r} = \Sigma^{--} + \Sigma^{-+} \tag{4.78}$$

$$\Sigma^{a} = \Sigma^{--} + \Sigma^{+-} \tag{4.79}$$

We usually work with the Fourier transformed Dyson's equation

$$\hat{G} = \hat{G}_o + \hat{G}_o\hat{\Sigma}\hat{G} \tag{4.80}$$

Because the Keldysh components are not linearly independent, we can choose to work with any three of them. The Dyson's equation for different components reads (detail see Appendix)

$$G^{A} = G_0^{A} + G_0^{A}\Sigma^{A}G^{A} \tag{4.81}$$

$$G^{R} = G_0^{R} + G_0^{R}\Sigma^{R}G^{R} \tag{4.82}$$

$$G^{+-} = (1 + \Sigma^{R}G^{R})G_0^{+-}(1 + \Sigma^{A}G^{A}) - G^{R}\Sigma^{+-}G^{A} \tag{4.83}$$

$$G^{-+} = (1 + \Sigma^{R}G^{R})G_0^{-+}(1 + \Sigma^{A}G^{A}) - G^{R}\Sigma^{-+}G^{A} \tag{4.84}$$

4.5 Langreth's Theorem

Langreth's theorem helps us to convert the contour integration into real time integration. One needs to evaluate products parallel or antiparallel in the time arguments

$$C_{\leftleftarrows}(\tau,\tau') = A(\tau,\tau')B(\tau,\tau') \tag{4.85}$$

$$C_{\leftrightarrows}(\tau,\tau') = A(\tau,\tau')B(\tau',\tau) \tag{4.86}$$

The $+-(-+)$ part corresponds to the particular ordering of the time arguments on the contour $\tau \in c+(c-)$ and $\tau' \in c-(c+)$. From the definition of $+-$ and $-+$ components:

$$C^{\lessgtr}_{\leftleftarrows}(t,t') = A^{\lessgtr}(t,t')B^{\lessgtr}(t,t') \tag{4.87}$$

$$C^{\lessgtr}_{\leftrightarrows}(t,t') = A^{\lessgtr}(t,t')B^{\gtrless}(t',t) \tag{4.88}$$

The compact representation of Langreth's theorem are collected in table below.

Contour	Real axis
$C = \int_c AB$	$C^{\lessgtr} = \int_t [A^r B \lessgtr + A \lessgtr B^a]$ $C^{r(a)} = \int_t A^{r(a)} B^{r(a)}$
$D = \iint_c ABC$	$D^{\lessgtr} = \iint_{t_1 t_2} [A^r B^r C^{\lessgtr} + A^r B^{\lessgtr} C^a + A^{\lessgtr} B^a C^a]$ $D^{r(a)} = \iint_{t_1\ t_2} A^{r(a)} B^{r(a)} C^{r(a)}$
$C_{\leftleftarrows}(\tau, \tau') = A(\tau, \tau') B(\tau, \tau')$	$C^{\lessgtr}_{\leftleftarrows}(t, t') = A^{\lessgtr}(t, t') B^{\lessgtr}(t, t')$ $C^r(t, t') = A^r(t, t') B^<(t, t') + A^<(t, t') B^r(t, t')$ $\quad + A^r(t, t') B^r(t, t')$ $C^a(t, t') = A^a(t, t') B^<(t, t') + A^<(t, t') B^a(t, t')$ $\quad - A^a(t, t') B^a(t, t')$
$C_{\leftrightarrows}(\tau, \tau') = A(\tau, \tau') B(\tau', \tau)$	$C^{\lessgtr}_{\leftrightarrows}(t, t') = A^{\lessgtr}(t, t') B^{\gtrless}(t', t)$ $C^r(t, t') = A^r(t, t') B^<(t', t) + A^<(t, t') B^a(t', t)$ $C^a(t, t') = A^a(t, t') B^<(t', t) + A^<(t, t') B^a(t', t)$ $\quad - A^a(t, t') B^a(t, t')$

4.6 Information from Green's Functions

The diagonal element of $\tilde{G}$ characterizes the states of the quantum system, while the off-diagonal components contain information on the occupation of these states. This can be seen easily,considering, for instance, noninteracting electrons in equilibrium,with the Hamiltonian

$$H_0 = \sum_k \epsilon_k \ c_k^\dagger c_k$$

.The Fourier transformed Keldysh component is given by

$$G_k^{keld}(w) = -2\pi i (1 - 2f(\omega)) \delta(w - \epsilon_k) \tag{4.89}$$

where $f(\epsilon_k)$ is the statistical distribution function,either the Fermi Dirac $n_F(\omega-\mu) = (e^{\beta(\omega-\mu)}+1)^{-1}$ for fermions or the Bose-Einstein $n_B(\omega) = (e^{\beta\omega}-1)^{-1}$. Once we know the G^{keld}, the distribution function can be calculated:

$$f(\omega) = \frac{1}{2} + \int \frac{d\omega}{2\pi i} G_k^{keld}(\omega) \tag{4.90}$$

In steady state non-equilibrium problem, there are two independent Green's functions. In equilibrium situation, some further relations are:[84]

$$G^{+-}(\omega) = \pm i f(\omega) A(\omega) \tag{4.91}$$

$$G^{-+}(\omega) = i[\pm f(\omega) - 1] A(\omega) \tag{4.92}$$

where $A(\omega)$ is the spectral function

$$\begin{aligned} A(\omega) &= i[G^r(\omega) - G^a(\omega)] \\ &= i[G^{-+}(\omega) - G^{+-}(\omega)] \end{aligned} \tag{4.93}$$

The upper sign in front of $f(\omega)$ applies to fermions and lower sign to bosons.

One can understand the meaning of Green's functions with their physical interpretation. We have already seen that in equilibrium, the lesser Green's function G^{+-} is the energy resolved density of particles. It is the density of state $A(\omega)$ multiplied by $n_F(\omega)$, the statistical probability that these are occupied. In non-equilibrium situation, this multiplication relation doesn't hold, but the physical interpretation is always right. The G^{+-} contains the information about the distribution function and the density of states. Similarly,the greater Green's function, for instance in case of fermion, is the energy resolved density of holes.

The picture from the retarded Green's function is a vivid one. In the case of fermion, if one adds an extra particle at space-time (r_j, t_j), the retarded Green's function $G^r(i,j)$ tells us what's the probability that one is able to remove a particle at a later space-time (r_i, t_i). The retarded Green's function is defined for $t_i > t_j$, this assures it's causality. Actual systems are always causual. That's why we are interested in retarded Green's function. The Fourier transformed function $G^r(r_i, r_j, \omega)$ correspondingly tells the probability of adding one particle with energy ω at space r_j and removing another particle with energy ω at space r_i.

The advanced Green's function $G^a(i,j)$ interprets, on the other hand, how the hole excitation propagates. If we look at the definition of Spectral function, it is actually the combination of the retarded and advanced Green's function. It tells us that both the particles and hole excitations are involved in the physics. They are playing the same role in the system.

The Green's functions, besides having contained information in themselves, they are in fact related to physical observables. In principle, the ensemble average of any one-body operator $\mathcal{O}$ can be related to the Green's function[78]

$$\begin{aligned}\langle \mathcal{O}(r,t)\rangle &= T_r[\rho \mathcal{O}(r,t)] \\ &= T_r[\rho \Psi^\dagger_{\mathscr{H}}(r,t)\mathcal{O}(r,t)\Psi_{\mathscr{H}}(r,t)] \\ &= \lim_{r'\to r}\lim_{t'\to t} O(r,t) T_r[\rho \Psi^\dagger_{\mathscr{H}}(r',t')\Psi_{\mathscr{H}}(r,t)] \\ &= \lim_{r'\to r}\lim_{t'\to t} O(r,t)\langle \Psi^\dagger_{\mathscr{H}}(r',t')\Psi_{\mathscr{H}}(r,t)\rangle \\ &= \mp i\hbar \lim_{r'\to r}\lim_{t'\to t} O(r,t) G^{+-}(r't',rt)\end{aligned} \tag{4.94}$$

$O(r,t)$ is the operator in first quantization[78]. As an important example, let's consider the quantum average of the fermion particle density

$$\langle n(r,t)\rangle = -i\hbar \lim_{r'\to r}\lim_{t'\to t} G^{+-}(r't',rt) \tag{4.95}$$

It is obviously that the G^{+-} is related to particle density.

Chapter 5

Electron Conduction Band Coupled to Single Photon Mode

5.1 Introduction

People have been interested in plasmon physics. The fundamental point is the photon-electron interaction. How the photon-electron interaction will influence the electron states is an interesting problem. In this chapter, we are going to study electron conduction band coupled to a single photon mode. We introduce the coupling constant λ. We also consider the local coulomb-interaction between electrons and introduce its constant U. In the end it will be interesting to see the competition between the photon-electron interaction and the coulomb-interaction.

5.2 The Hamiltonian

We consider the following hamiltonian.

$$\begin{aligned} H = & \sum_{p\sigma} \epsilon_p c^\dagger_{p\sigma} c_{p\sigma} \ + \ \omega_0 \ a^\dagger a \\ & + \frac{U}{2\ V} \sum_{\substack{pp'\sigma\sigma' \\ q}} c^\dagger_{p+q\sigma} c^\dagger_{p'-q\sigma'} c_{p'\sigma'} c_{p\sigma} + \frac{\lambda}{\sqrt{V}} \sum_p c^\dagger_p c_p (a + a^\dagger) \end{aligned} \tag{5.1}$$

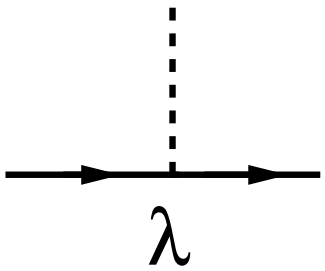

Figure 5.1: photon-electron interaction vertex. The full line is the electron's Green's function, the dash line is the photon's Green's funtion

ω_0 is the photon mode frequency. U is the constant for the electron coulomb interaction. We use λ for the coupling strength of photons to electon. V is the volume of the system

The first term of the hamiltonian describes a electron conduction band. $c^\dagger(c)$ is the electron creation(annihilation) operator.

The free electron density of state we are going to use is a smicircle

$$\rho(\epsilon_p) = \frac{2}{\pi D}\sqrt{1-(\frac{\epsilon_p}{D})^2} \tag{5.2}$$

where ϵ_p is the energy of electron, and D is the half bandwidth. The second term describes a single photon mode, where $a^\dagger(a)$ is the photon creation(annihilation) operator. Electron coulomb interaction is considered by the third term. In the last term, we couple the electron with the photon.

We are going to do perturbation theory to solve the problem. A graphical representation of the photon-electron vertex is illustrated in Figure5.1.

5.3 Definition of Green's function

We define Green's function components in the Keldysh space for electrons

$$G^{+-}(p,t_1,t_2) = \ i < c_p^\dagger(t_2)c_p(t_1) > \tag{5.3}$$

$$G^{-+}(p,t_1,t_2) = \ -i < c_p(t_1)c_p^\dagger(t_2) > \tag{5.4}$$

$$G^{ret}(p,t_1,t_2) = \ \theta(t_1-t_2)[G^{>}(p,t_1,t_2) - G^{<}(p,t_1,t_2)] \tag{5.5}$$

$$G^{adv}(p,t_1,t_2) = \ -\theta(t_2-t_1)[G^{>}(p,t_1,t_2) - G^{<}(p,t_1,t_2)] \tag{5.6}$$

For photons we have

$$D^{+-}(t_1,t_2) = \ i < A(t_2)A(t_1) > \tag{5.7}$$

$$D^{-+}(t_1,t_2) = \ i < A(t_1)A(t_2) > \tag{5.8}$$

$$D^{ret}(t_1,t_2) = \ \theta(t_1-t_2)[D^{-+}(t_1,t_2) - D^{+-}(t_1,t_2)] \tag{5.9}$$

$$D^{adv}(t_1,t_2) = \ -\theta(t_2-t_1)[D^{-+}(t_1,t_2) - D^{+-}(t_1,t_2)] \tag{5.10}$$

where $A(t) = a(t) + a^{\dagger}(t)$.

5.4 Useful Relations

Usually we will work with the Fourier-transfered Green's function. There are some relationship:

$$G^{ret}(\omega) = [G^{adv}(\omega)]^{\dagger} \tag{5.11}$$

$$D^{ret}(\omega) = [D^{adv}(\omega)]^{\dagger} \tag{5.12}$$

The spectral funtions of electrons and photons are defined:

$$\Gamma(\omega) = \ i[G^{ret}(\omega) - G^{adv}(\omega)] \tag{5.13}$$

$$B(\omega) = \ i[D^{ret}(\omega) - D^{adv}(\omega)] \tag{5.14}$$

There are also relationships between various self-energies that we are going to use later

$$i[\Sigma^{-+}(\omega) - \Sigma^{+-}(\omega)] = i[\Sigma^{ret}(\omega) - \Sigma^{adv}(\omega)] = \Delta(\omega) \tag{5.15}$$

and

$$\Sigma^{ret}(\omega) = \ P\int \frac{d\omega'}{\pi}\frac{\Delta(\omega')}{\omega-\omega'} - \frac{i}{2}\Delta(\omega) \tag{5.16}$$

These relations are valid for both boson and fermion.

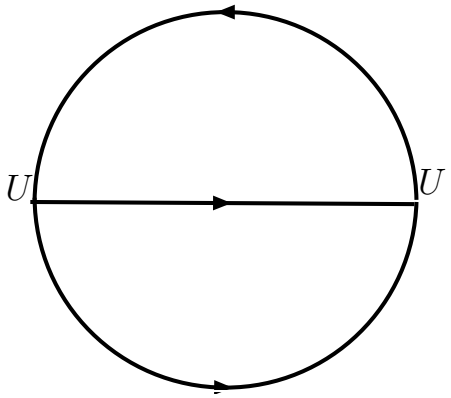

Figure 5.2: Selfenergy diagram for electron from coulomb interaction

5.5 Electron Selfenergy

After doing the second order perturbation expandsion, there are two self energy diagrams to be calculated for the electron self-energy. One is the diagram for photon-electron interaction, the other one comes from the coulomb interaction. We will apply local approximation to calculate the coulomb interaction self-energy. Therefore the coulomb interaction self-energy will be momentum independent.

5.5.1 Contribution from Coulomb Interaction

Figure5.2 represents the second order diagram for coulomb interaction. Now we calculate it with keldysh Green's Function.

$$\Sigma^{+-}_{coulomb}(\omega) = U^2 \int_{-\infty}^{\infty} \frac{d\omega_1}{2\pi} \int_{-\infty}^{\infty} \frac{d\omega_2}{2\pi} G^{+-}(\omega_1 + \omega_2) G^{+-}(\omega - \omega_2) G^{-+}(\omega_1) \tag{5.17}$$

$$\Sigma^{-+}_{coulomb}(\omega) = U^2 \int_{-\infty}^{\infty} \frac{d\omega_1}{2\pi} \int_{-\infty}^{\infty} \frac{d\omega_2}{2\pi} G^{-+}(\omega_1 + \omega_2) G^{-+}(\omega - \omega_2) G^{+-}(\omega_1) \tag{5.18}$$

In order to write them in a compacter form,we define the distribution functions

$$f^{+-}(\omega) = -\frac{G^{+-}(\omega)}{2i\Im G^{ret}(\omega)} \tag{5.19}$$

$$f^{-+}(\omega) = \frac{G^{-+}(\omega)}{2i\Im G^{ret}(\omega)} \tag{5.20}$$

We also define

$$\Xi(\omega) = \frac{\Im G^{ret}(\omega)}{\pi} \tag{5.21}$$

Then we can write the selfenergy as

$$\begin{aligned}\Sigma^{+-}_{coulomb}(\omega) =& 2\pi U^2 \int_{-\infty}^{\infty} \frac{d\epsilon_1}{\pi} \int_{-\infty}^{\infty} \frac{d\epsilon_2}{\pi} \Xi(\epsilon_1)\Xi(\epsilon_2)\Xi(\epsilon_1+\epsilon_2-\omega) \\ & f^{+-}(\epsilon_1)f^{+-}(\epsilon_2)f^{-+}(\epsilon_1+\epsilon_2-\omega)\end{aligned} \tag{5.22}$$

$$\begin{aligned}\Sigma^{-+}_{coulomb}(\omega) =& -2\pi U^2 \int_{-\infty}^{\infty} \frac{d\epsilon_1}{\pi} \int_{-\infty}^{\infty} \frac{d\epsilon_2}{\pi} \Xi(\epsilon_1)\Xi(\epsilon_2)\Xi(\epsilon_1+\epsilon_2-\omega) \\ & f^{-+}(\epsilon_1)f^{-+}(\epsilon_2)f^{+-}(\epsilon_1+\epsilon_2-\omega)\end{aligned} \tag{5.23}$$

where,

$$f^{-+}(\omega) = \frac{G^{-+}(\omega)}{2i\Im G^{ret}(\omega)} \quad f^{+-}(\omega) = \frac{G^{+-}(\omega)}{2i\Im G^{ret}(\omega)} \tag{5.24}$$

Unter Gleichgewicht,$f^{+-}(\omega) = n_F(\omega)$ and $f^{-+}(\omega) = 1 - n_F(\omega)$

Then the imaginary part of the retarded selfenergy can be written as

$$\Im\Sigma^{ret}_{coulomb}(\omega) = -\frac{1}{2}\{\Sigma^{-+}_{coulomb}(\omega) - \Sigma^{+-}_{coulomb}(\omega)\}$$

$$\begin{aligned}\Sigma^{ret}_{coulomb}(\omega) =& 2\pi U^2 \int_{-\infty}^{\infty} \frac{d\epsilon_1}{\pi} \int_{-\infty}^{\infty} \frac{d\epsilon_2}{\pi} \Xi(\epsilon_1)\Xi(\epsilon_2)\Xi(\epsilon_1+\epsilon_2-\omega) \\ & \{f^{+-}(\epsilon_1)f^{+-}(\epsilon_2)f^{-+}(\epsilon_1+\epsilon_2-\omega) \\ & - f^{-+}(\epsilon_1)f^{-+}(\epsilon_2)f^{+-}(\epsilon_1+\epsilon_2-\omega)\}\end{aligned} \tag{5.25}$$

As a special case, these expression have simplified forms unter two conditions. One is equilibrium, the other is zero temperature. If conditions are fullfilled, then we have

$$T \to 0K \qquad f^{+-}(\omega) = \theta(-\omega) \tag{5.26}$$

where the θ function is defined as

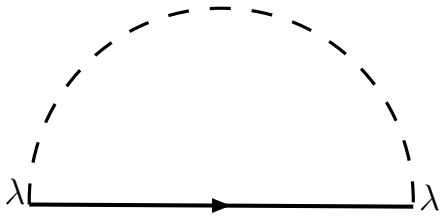

Figure 5.3: Electron selfenergy diagram from photon-electron interaction

$$\theta(x) = \begin{cases} 1 & \text{if } x > 0 \\ \frac{1}{2} & \text{if } x = 0 \\ 0 & \text{if } x < 0 \end{cases}$$

Then under the assumption that $T = 0K$ we have

$$\Sigma^{+-}_{coulomb}(\omega) = 2\pi U^2 \int_{\omega}^{0} \frac{d\epsilon_1}{\pi} \int_{\omega-\epsilon_1}^{0} \frac{d\epsilon_2}{\pi}\ \Xi(\epsilon_1)\Xi(\epsilon_2)\Xi(\epsilon_1+\epsilon_2-\omega) \qquad \omega < 0 \tag{5.27}$$

$$\Sigma^{-+}_{coulomb}(\omega) = -2\pi U^2 \int_{0}^{\omega} \frac{d\epsilon_1}{\pi} \int_{0}^{\omega-\epsilon_1} \frac{d\epsilon_2}{\pi}\ \Xi(\epsilon_1)\Xi(\epsilon_2)\Xi(\epsilon_1+\epsilon_2-\omega) \qquad \omega > 0 \tag{5.28}$$

The retard selfenergy in this case reads

$$\Sigma^{ret}_{coulomb}(\omega) = -2\pi U^2 \int_{0}^{\omega} \frac{d\epsilon_1}{\pi} \int_{0}^{\omega-\epsilon_1} \frac{d\epsilon_2}{\pi}\ \Xi(\epsilon_1)\Xi(\epsilon_2)\Xi(\epsilon_1+\epsilon_2-\omega) \tag{5.29}$$

5.5.2 Contribution from Photon-Electron Interaction

Self-energy from photon-electron interaction is calculated according to the diagram showed in Figure5.3.

$$\Sigma^{+-}_{pho-elec}(\epsilon_p, \omega) = \lambda^2 \int \frac{d\tilde{\omega}}{2\pi} G^{+-}(\epsilon_p, \tilde{\omega}+\omega) D^{-+}(\tilde{\omega}) \tag{5.30}$$

$$\Sigma^{-+}_{pho-elec}(\epsilon_p, \omega) = \lambda^2 \int \frac{d\tilde{\omega}}{2\pi} G^{-+}(\epsilon_p, \tilde{\omega}+\omega) D^{+-}(\tilde{\omega}) \tag{5.31}$$

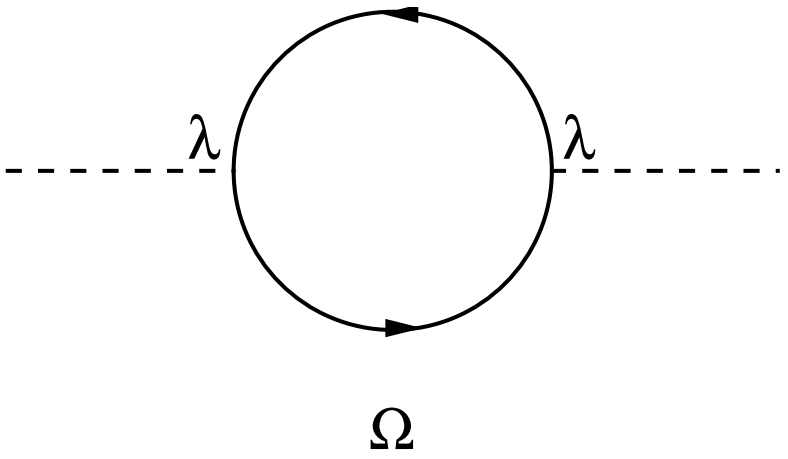

Figure 5.4: Selfenergy diagram for photon from photon-electron interaction

Again the retarded part can be calculated with the less and larger part

$$\Im\Sigma^{ret}_{pho-elec}(\epsilon_p,\omega) = \frac{i}{2}\{\Sigma^{-+}_{pho-elec}(\epsilon_p,\omega) - \Sigma^{+-}_{pho-elec}(\epsilon_p,\omega)\} \tag{5.32}$$

5.6 Photon Selfenergy

The selfenergy for photons comes from the Bubble diagram, see figure5.4. It is in fact the plasmon. In this way, the photons are coupled to electrons and obtain self-energy from the plasmon. For the electron lines in the Bubble diagram, we use the local Green's function to calculate

$$\Omega^{+-}(\omega) = -\lambda^2 \int \frac{d\tilde{\omega}}{2\pi} G^{+-}(\tilde{\omega}+\omega)G^{-+}(\tilde{\omega}) \tag{5.33}$$

$$\Omega^{-+}(\omega) = -\lambda^2 \int \frac{d\tilde{\omega}}{2\pi} G^{-+}(\tilde{\omega}+\omega)G^{+-}(\tilde{\omega}) \tag{5.34}$$

$$\Im\Omega^{ret}(\omega) = \frac{i}{2}\{\Omega^{-+}(\omega) - \Omega^{+-}(\omega)\} \tag{5.35}$$

5.7 Self-consistent Theory

In order to solve this problem numerically, we are going to set up a self-consistent process. We calculate the physical quantities iteratly until a stable

solution is found.

It is the dyson's equation that connects the selfenergy to their full Green's function. In the previous chapter, we have discussed the dyson's equation for different components in Keldysh space.

$$G^R = G_0^R + G_0^R \Sigma^R G^R$$

$$G^{+-} = (1 + \Sigma^R G^R) G_0^{+-} (1 + \Sigma^A G^A) - G^R \Sigma^{+-} G^A$$

$$G^{-+} = (1 + \Sigma^R G^R) G_0^{-+} (1 + \Sigma^A G^A) - G^R \Sigma^{-+} G^A$$

These equations are also valid to the photon Green's function. In the retarded component to the electrons, we have

$$\Sigma^{ret}(\epsilon_p, \omega) = \Sigma^{ret}_{coulomb}(\omega) + \Sigma^{ret}_{pho-elec}(\epsilon_p, \omega) \tag{5.36}$$

We define electron free Green's function,

$$G_0^{ret}(\epsilon_p, \omega) = \frac{1}{\omega - \epsilon_p + i\eta} \tag{5.37}$$

Then using dyson's equation we can calculate the full Green's function $G^{ret}(\epsilon, \omega)$ Then we can solve the full local retarded Green's function out of the dyson's equation

$$G^{ret}(\epsilon_p, \omega) = \frac{1}{\omega - \epsilon_p - \Sigma(\epsilon_p, \omega)} \tag{5.38}$$

Then we can calculate the local retarded Green's function:

$$G^{ret}(\omega) = \int_{-D}^{D} d\epsilon_p \rho(\epsilon) \frac{1}{\omega - \epsilon_p - \Sigma(\epsilon_p, \omega)} \tag{5.39}$$

The imaginary part of full local retarded Green's function is

$$\Im G^{ret}(\omega) = \int_{-D}^{D} d\epsilon_p \rho(\epsilon_p) \frac{\Im \Sigma^{ret}(\omega)}{(\omega - \epsilon_p - \Re \Sigma^{ret}(\omega))^2 + \Im \Sigma^{ret}(\omega)^2} \tag{5.40}$$

where ρ is given at the beginning of this chapter. It is easy to see, the free local retarded Green's function is

$$\Im G_0^{ret}(\omega) = -\pi \rho(\omega) \tag{5.41}$$

Now we come to the components G^{+-} and G^{-+}. As soon as we introduce interaction, under the assumption of a homogeneous and steady system, the first term on the right side of the dyson's equation for G^{+-} and G^{-+} will be zero. Only the second term survives.

$$G^{+-}(\epsilon_p,\omega) = G^{ret}(\epsilon_p,\omega)\Sigma^{+-}(\epsilon_p,\omega)G^{adv}(\epsilon_p,\omega) \tag{5.42}$$

$$G^{-+}(\epsilon_p,\omega) = G^{ret}(\epsilon_p,\omega)\Sigma^{-+}(\epsilon_p,\omega)G^{adv}(\epsilon_p,\omega) \tag{5.43}$$

and the local Green's function are:

$$\begin{aligned} G^{+-}(\omega) &= -\int_{-D}^{+D} d\epsilon_p \rho(\epsilon_p)\; G^{ret}(\epsilon_p,\omega)\Sigma^{+-}(\epsilon_p,\omega)G^{adv}(\epsilon_p,\omega) \\ &= -\int_{-D}^{D} d\epsilon_p \rho(\epsilon_p) \frac{\Sigma^{+-}(\epsilon_p,\omega)}{(\omega-\epsilon-\Re\Sigma^{ret}(\epsilon_p,\omega))^2+\Im\Sigma^{ret}(\epsilon_p,\omega)^2} \end{aligned} \tag{5.44}$$

$$\begin{aligned} G^{-+}(\omega) &= -\int_{-D}^{+D} d\epsilon_p \rho(\epsilon_p)\; G^{ret}(\epsilon_p,\omega)\Sigma^{-+}(\epsilon_p,\omega)G^{adv}(\epsilon_p,\omega) \\ &= -\int_{-D}^{D} d\epsilon_p \rho(\epsilon_p) \frac{\Sigma^{-+}(\epsilon_p,\omega)}{(\omega-\epsilon-\Re\Sigma^{ret}(\epsilon_p,\omega))^2+\Im\Sigma^{ret}(\epsilon_p,\omega)^2} \end{aligned} \tag{5.45}$$

Similarly to the retarded one, selfenergy components $\Sigma^{+-}(\omega)$ and $\Sigma^{-+}(\omega)$ consist of two contributions

$$\Sigma^{+-}(\epsilon_p,\omega) = \Sigma^{+-}_{coulomb}(\omega) + \Sigma^{+-}_{pho-elec}(\epsilon_p,\omega) \tag{5.46}$$

$$\Sigma^{-+}(\epsilon_p,\omega) = \Sigma^{-+}_{coulomb}(\omega) + \Sigma^{-+}_{pho-elec}(\epsilon_p,\omega) \tag{5.47}$$

The free retarded Green's function of photon is:

$$D_0^{ret}(\omega) = \frac{1}{\omega-\omega_0+i\eta} - \frac{1}{\omega+\omega_0-i\eta} \tag{5.48}$$

The photon retarded Green reads

$$D^{ret}(\omega) = \frac{1}{\frac{\omega^2-\omega_0^2}{2\omega_0} - \Omega^{ret}(\omega)} \tag{5.49}$$

We are interested mostly in the imaginary part of the Green's function

$$\Im D^{ret}(\omega) = \frac{\Im\Omega^{ret}(\omega)}{\{\frac{\omega^2-\omega_0^2}{2\omega_0} - \Re\Omega^{ret}(\omega)\}^2 + \Im\Omega^{ret}(\omega)^2} \tag{5.50}$$

We now treat the problem as a steady and homogeneous problem, it is necessary to give it a boundary condition. A suitable position to introduce the boundary condition is to define the laser distribution function.

$$n_L(\omega) = \frac{W}{\sqrt{2\pi\sigma}} \left(e^{-\frac{(\omega-\omega_0)^2}{2\sigma^2}} - e^{-\frac{(\omega+\omega_0)^2}{2\sigma^2}} \right) \tag{5.51}$$

the parameter σ controls the laser width in the frequency domain.

With the boundary condition, the unperturbed less und larger Green's functions for photon are found to be

$$D_0^{+-/-+}(\omega) = 2i\ n_L(\omega)\Im D_0^{ret}(\omega) \tag{5.52}$$

and the full Green's function:

$$D^{+-/-+}(\omega) = 2i\ n_L(\omega)\Im D^{ret}(\omega) \tag{5.53}$$

So far, we have developed the equations for each component of Green's function in the Keldysh space and the equations for selfenergy. They can be calculate self-consistently. In the next chapter, we will discuss the numerical implementation.

Chapter 6

Numerical Implementation

6.0.1 Introduction

In the previous chapter, we have set up a self-consistent theory for the problem. This chapter concerns about the numerical implementation.

We have chosen the C programming language. The C programming language uses a straightforward compiler, to provide low-level access to memory. It can provide language constructs that map efficiently to machine instructions, requires minimal run-time support.

In order to find the self-consistent solution, one has to calculate the Green's function and selfenergy iterately until the results converge. First of all, we set our parameters and boundary conditions, then we calculate the Keldysh selfenergy components. With the selfenergies, we can again calculate the corresponding Green's functions. This will be done until the selfenergy and Green's functions don't change anymore. Figure 6.1 show the iterative procedure.

6.0.2 Program Structure

At the beginning of the calculation, one sets up the parameters for the system. This includes the conduction band structure. We choose for the electrons the free density of states to be $\rho(\epsilon) = \frac{2}{\pi D}\sqrt{1-(\frac{\epsilon}{D})^2}$. For convenience, we are going to choose D to be the unit. We will measure other quantities with respect to the half bandwidth. Variables are constant U for the electron coulomb interaction, and the constant λ for photon-electron interaction. One of the interesting point is to look at the competition between U and λ.

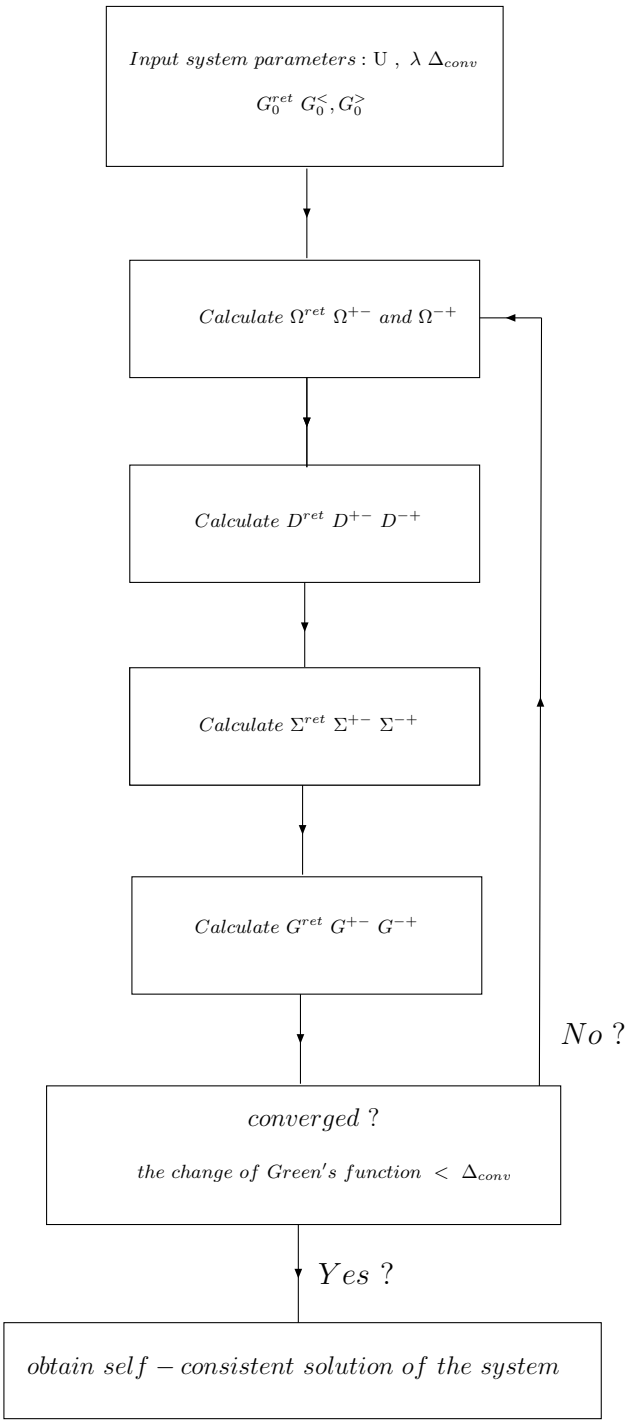

Figure 6.1: Block diagram illustrating the iterative procedure

With the free density of states, we can initiate the Green's functions for electrons: G^{ret} , G^{+-} and G^{-+}. By using Eq.(4.33),Eq.(4.34) and Eq.(4.35) one can calculate the retarded selfenergy for photons. Then with Eq.(4.30), Eq.(4.31) and Eq.(4.32), the selfenergy from photon-electron interaction can be calculated. Meanwhile, one calculates for electrons the selfenergy due to the coulomb interaction.One has to notice that the selfenergy for electrons consists of two parts. They are to be calculated separately. Remember that

$$\Sigma^{+-}(\omega) = \Sigma^{+-}_{coulomb}(\omega) + \Sigma^{+-}_{pho-elec}(\omega)$$

$$\Sigma^{-+}(\omega) = \Sigma^{-+}_{coulomb}(\omega) + \Sigma^{-+}_{pho-elec}(\omega)$$

$$\Im\Sigma^{ret}(\omega) = \frac{i}{2}(\Sigma^{-+}(\omega) - \Sigma^{+-}(\omega))$$

The real part of the Σ can be calculated using Kramers-Kronig relation, see Appendix

$$\Re\Sigma^{ret}(\omega) = \frac{1}{\pi}\mathcal{P}\int_{-\infty}^{\infty} d\omega' \frac{\Im\Sigma(\omega')}{\omega' - \omega} \tag{6.1}$$

With the selfenergy, one can evaluate the full Green's function. Then the pointer comes to the evaluation of photon selfenergy again, and so on. The iteration will go on until the criterion Δ_{conv} is fullfilled. In the programm we set Δ_{conv} to be $10^{-4}\%$, which means the fluctuation of Green's function is less than $10^{-4}\%$.

Chapter 7

Results and Discussion

In the previous chapters, we have present a model, which describes single photon mode with non-equilibrium laser distribution interacting with a electron conduction band. In this model, there are two important parameter: U and W. U is the parameter to define the coulomb-interaction strength. W controls the laser intensity. Numerical results will be shown in the following order: Firstly set $U = 0$, treat the electron as free particle, vary the laser intensity to see what the laser can do to the electron spectral function. Secondly we switch on the U parameter. The competition between U and W are going to be interesting. All the results are calculated under zero temperature. Remember our laser distribution function:

$$n_L(\omega) = \frac{W}{\sqrt{2\pi\sigma}} \left(e^{-\frac{(\omega-\omega_0)^2}{2\sigma^2}} - e^{-\frac{(\omega+\omega_0)^2}{2\sigma^2}} \right) \tag{7.1}$$

7.1 Situation $U = 0$

As soon as the single laser mode is coupled with electron band, fano resonance occurs in electron density of states. The larger is the laser intensity, the stronger is the fano resonance (Fig7.1 and Fig7.2). The resonance structure occurs exactly at the laser mode frequency. Fig 7.2 is the zoom-in of Fig 7.1, the laser frequency is 0.3, in the unit of half conduction band width. At large laser intensity, even the higher order resonance structure can be recognize.

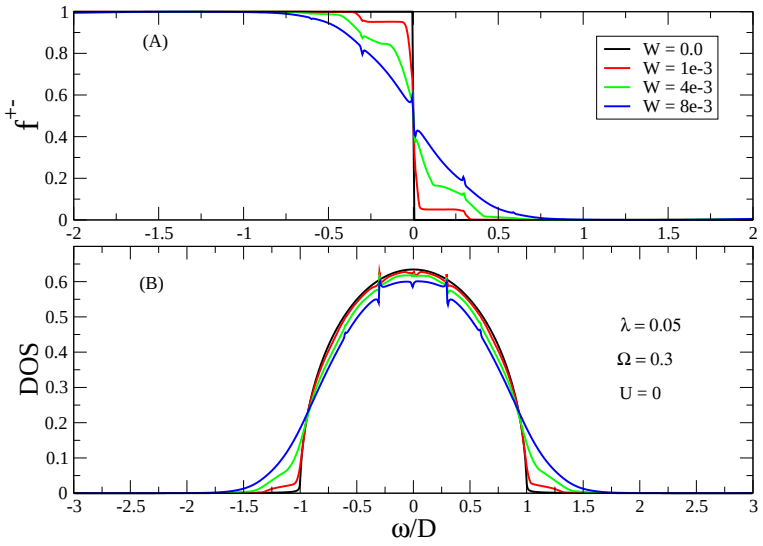

Figure 7.1: (A) Electron distribution function (B) Electron DOS, as function of frequency. Unit: half bandwidth

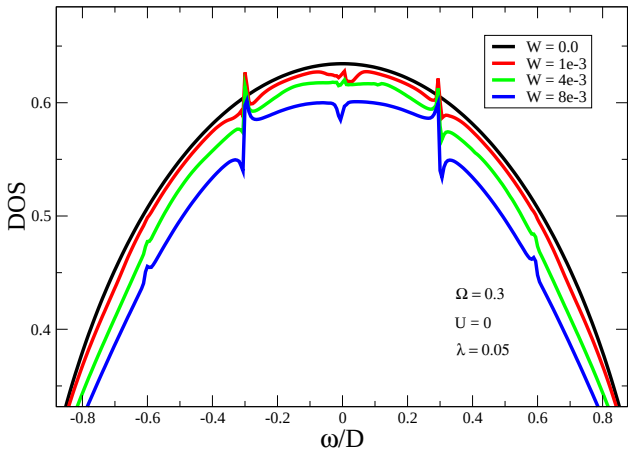

Figure 7.2: Electron DOS as function of frequency, Unit: half bandwidth.

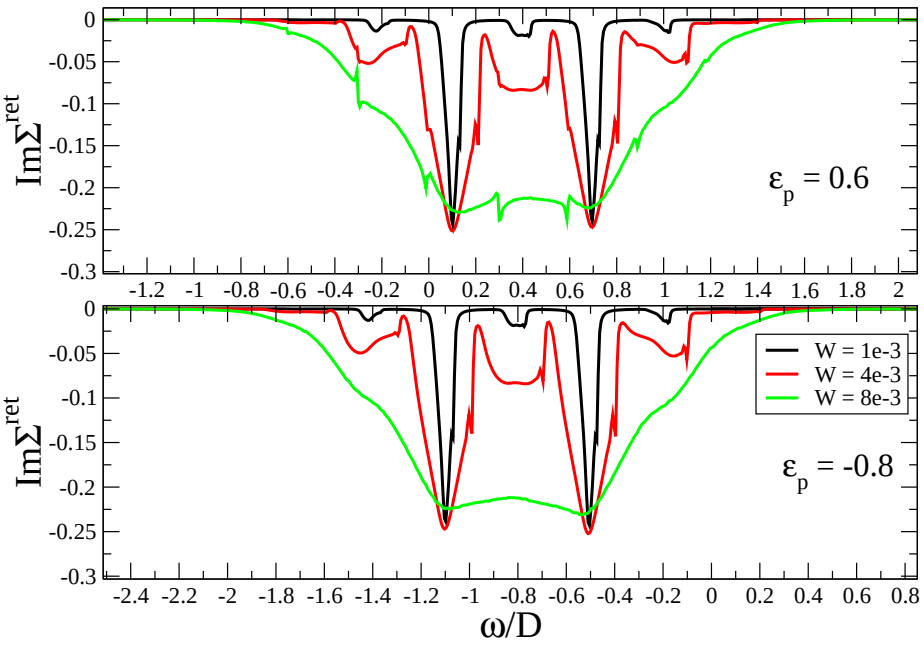

Figure 7.3: Electron retarded self-energy from photon-electron interaction

Parallel to the fano resonance in DOS, the fermi edge in the electron distribution function is changed by the laser, we observe clear harmonic effect at the the laser frequency (Fig 7.1(A)).

In the self-energy graph (Fig 7.3), the laser arouses two resonance peaks, whose distance is nothing else but the laser frequency. As the intensity becomes larger, the gap between those two peak gradually diminish (see the green line in Fig 7.3). The trend suggests that over-strong laser might wash out the resonance structure as well.

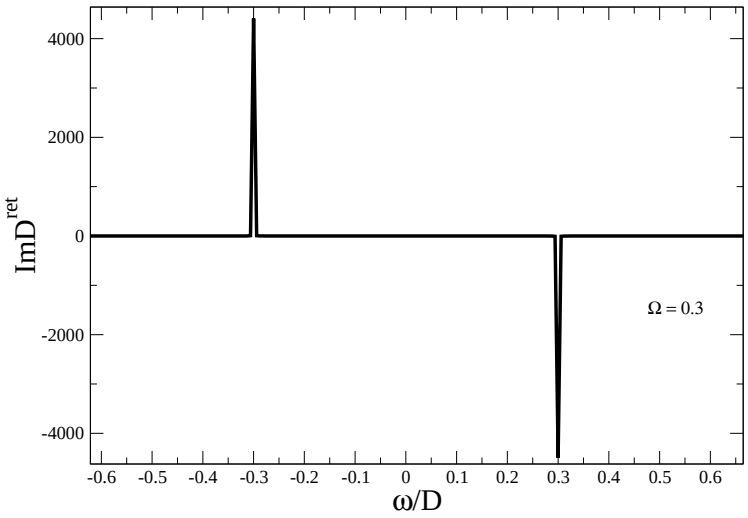

Figure 7.4: Imaginary part of photon retarded Green's Function

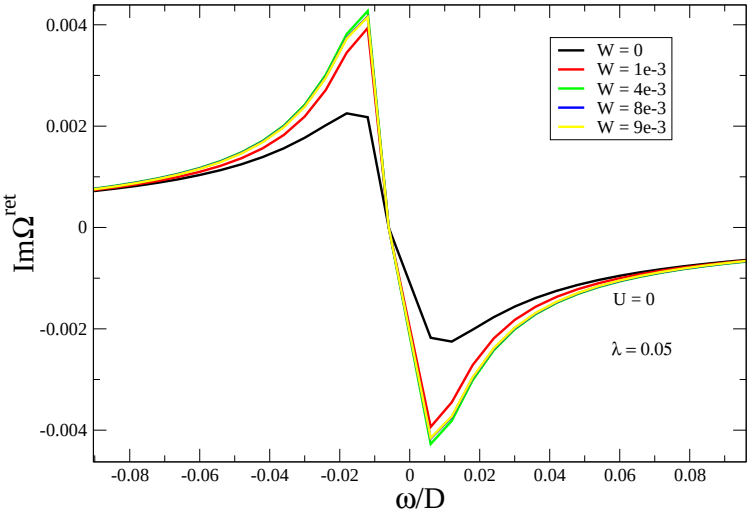

Figure 7.5: Imaginary part of photon retarded self-energy

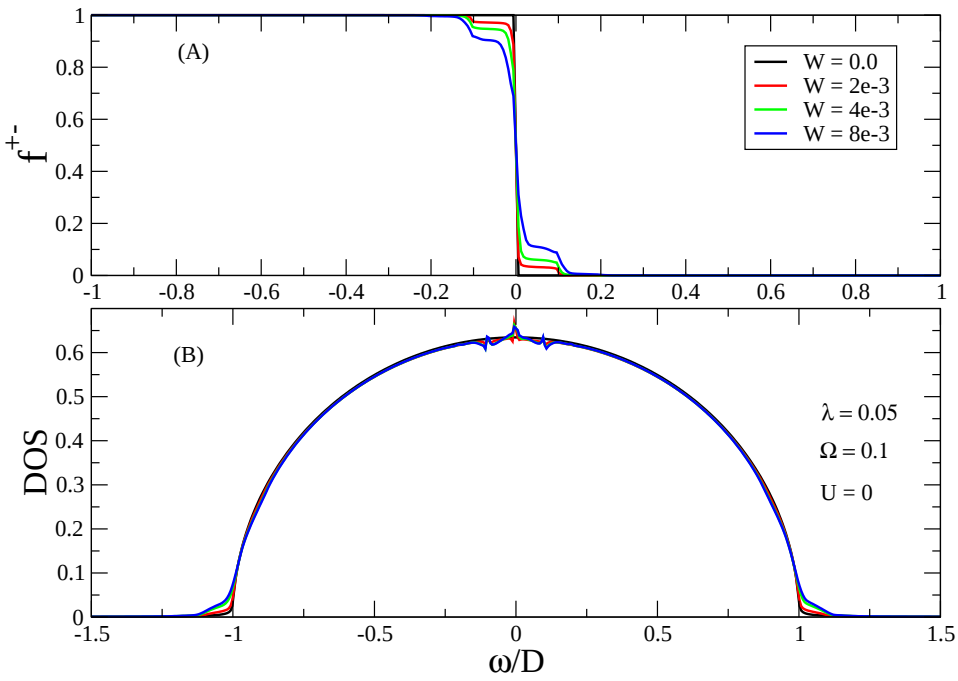

Figure 7.6: Electron density of state , $\Omega = 0.1$

In Fig 7.4, it shows the imaginary part of photon retarded Green's Function, also tells about the photon spetrum function. The photon mode frequency is 0.3 of the half bandwidth. We can see, the photon spetrum function has two sharp peaks located at plus and minus photon mode frequency. If one changes the photon mode frequency, the location of those peaks will also be shifted.

The photon self-energy is asymmetric at the frequency domain (Fig 7.5). Photon self-energy is calculated from the bubble diagram, this diagram is essentially the plasom. From Fig 7.5, we see the amplitude of photon self-energy des not monotonically increase with the laser intensity. That suggusts the plasom can be disturbed by strong nonequilibrium photon field, leading to optical properties variation.

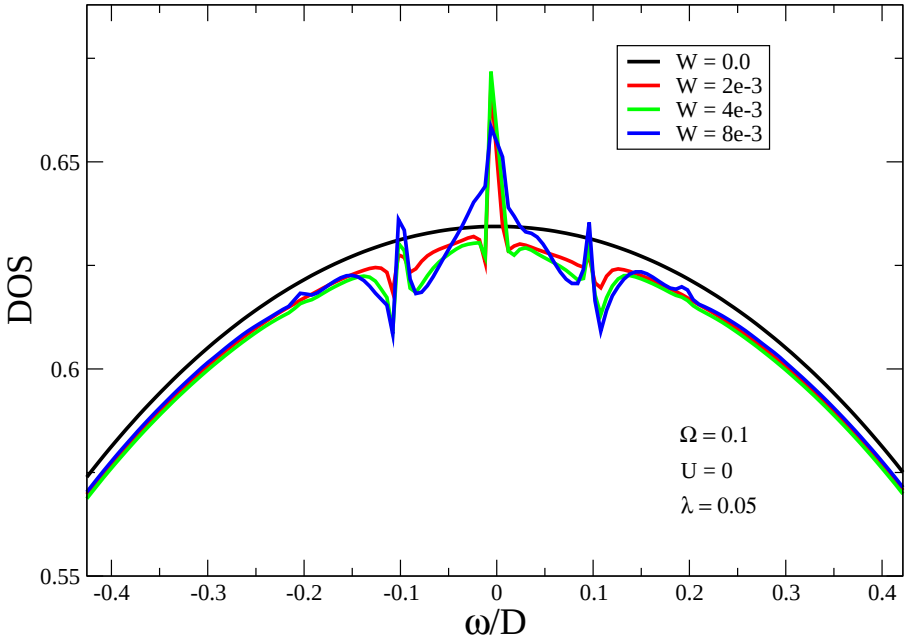

Figure 7.7: Electron density of state , $\Omega = 0.1$

Now we change the photon mode frequency to 0.1, see Fig 7.6 and Fig 7.6. The laser mode frequency is now 0.1, the position of fano resonance is correspondingly shifted. This is also true with the harmonic effect in the distribution function (Fig 7.6).

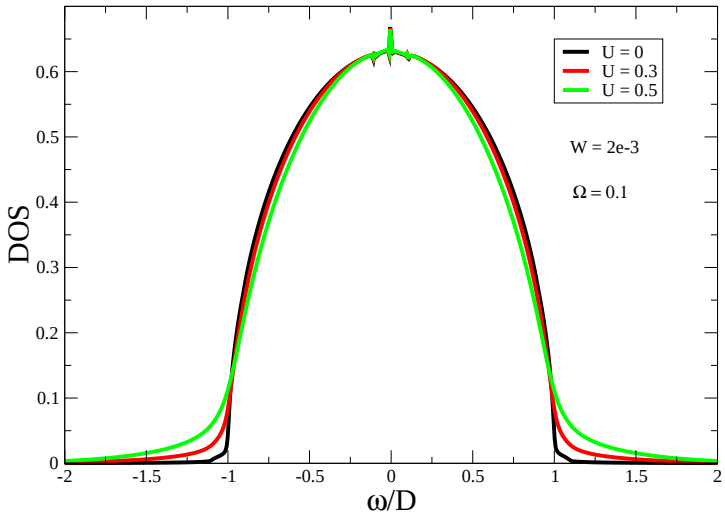

Figure 7.8: Electron DOS under different U, $\Omega = 0.1$

7.2 Situation $U \neq 0$

Now we turn on the electron coulomb interaction U.

We can see from Fig 7.8 and Fig 7.9 (zoom in of Fig 7.8), the electron coulomb interaction causes damping to the resonance structure. Let's look at another example. In Fig 7.10 and Fig 7.10 (Fig 7.10) , this phenomenon is very obvious to see. It tells us, the coulomb interaction tends to prevent the laser field from arising resonance structure to electron density of state. Let's also look at the electron distribution function. For $U = 0$, we can see only the electron whose absolute energy value less than laser mode frequency are pumped to above fermi surface. But as U increases, the electrons can exchange energy through coulomb interaction. The electrons are easier to be pumped with large U value. On the other hand, the coulomb interaction are destroying the resonance effects.

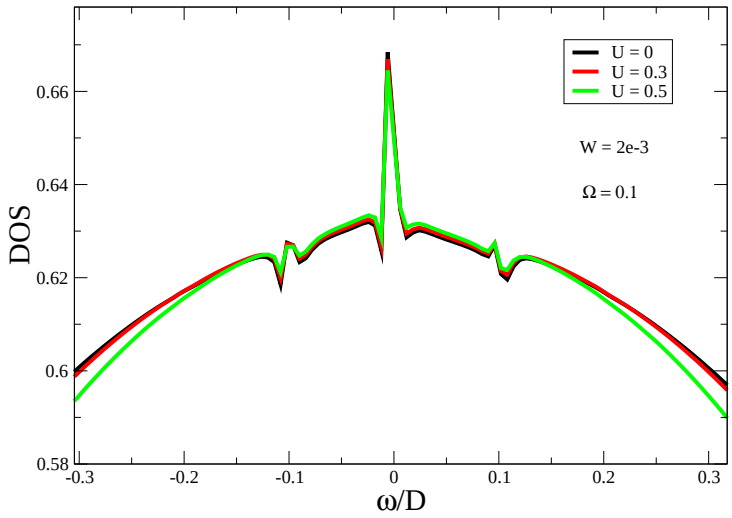

Figure 7.9: Electron DOS under different U, $\Omega = 0.1$

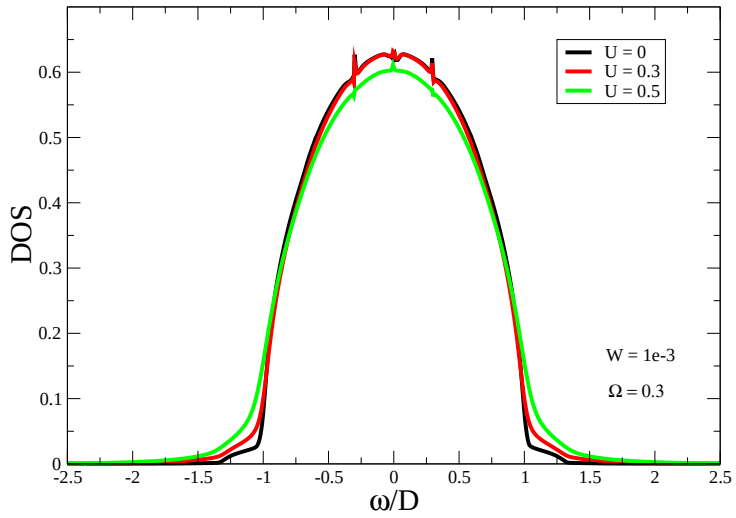

Figure 7.10: Electron DOS under different U, $\Omega = 0.3$

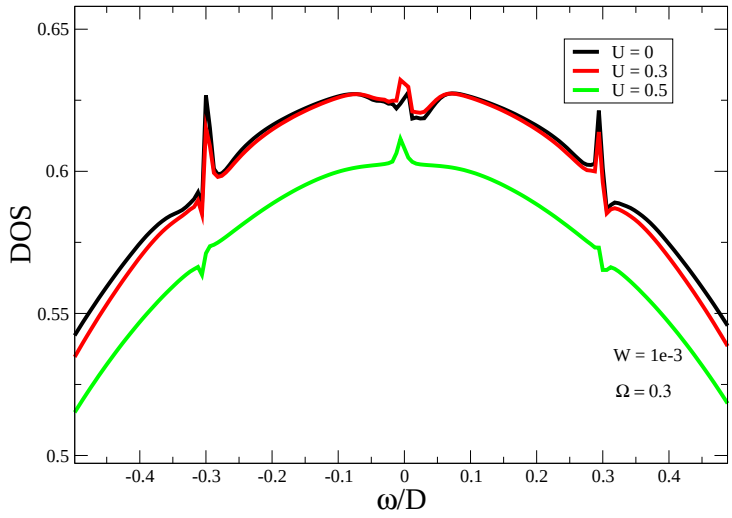

Figure 7.11: Electron DOS under different U, $\Omega = 0.3$

In Fig 7.13, we can see the peaks in eletron retarded self-energy are damped as the U increases. That is the reason why the resonance effects in electron DOS are damped. We can explain this with the electron spetral function. For near-free-electron system, the electron spectral function for each momentum is sharp peak in frequency domain. Then when coulomb interaction comes up, the width of electron spectral functions are boardened. The electron spectral functions are coupled to the photon field to contribute to the electron self-energy, leading to the peak-boardening in self-energy.

The coulomb interaction also contributes to the electron self-energy, see Fig 7.14. In equilibrium ($W = 0$), $\Sigma^{ret}_{coulomb}(\omega)$ has quadratic behavior $\sim \omega^2$ in the vicinity of zero, see the black curve in Fig 7.14. At the presence of laser field, the curve in the vicinity of zero frequency grows up. That is due to the coulomb interaction contributed from the excited electron above the fermi edge.

From Fig 7.15, one can see again, the amplitude of photon self-energy does not monotonically increases with the laser intensity. This agrees with the result in Fig 7.5, which is without coulomb interaction.

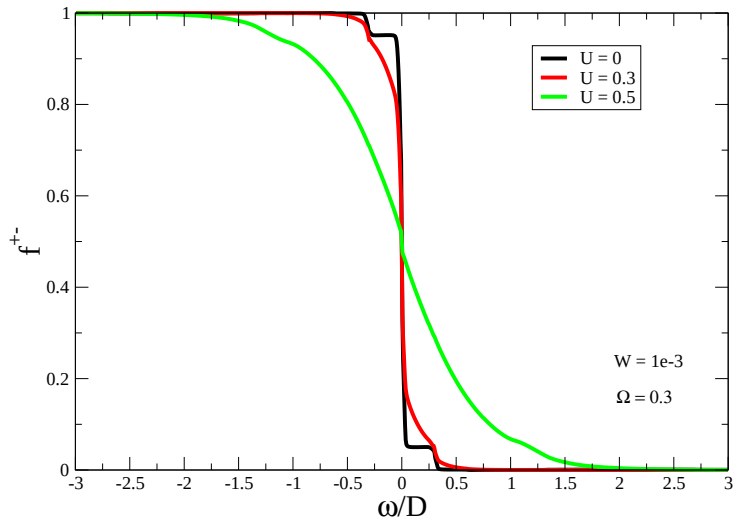

Figure 7.12: Electron distribution function under different U

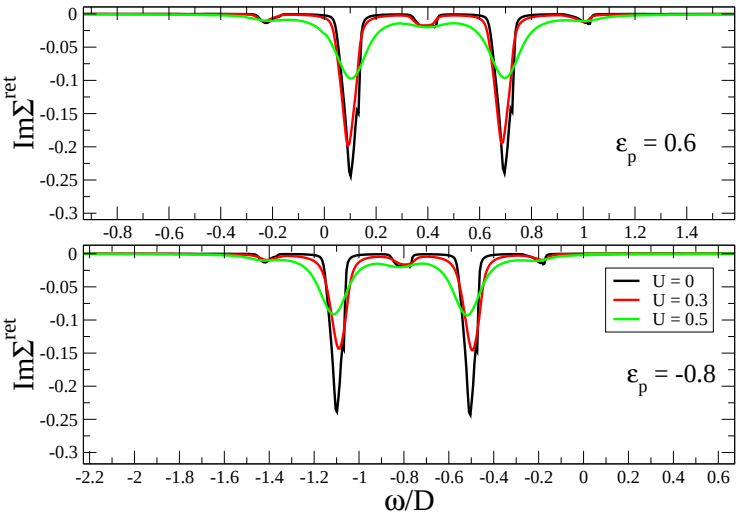

Figure 7.13: Electron retard self-energy from photon-electron interaction

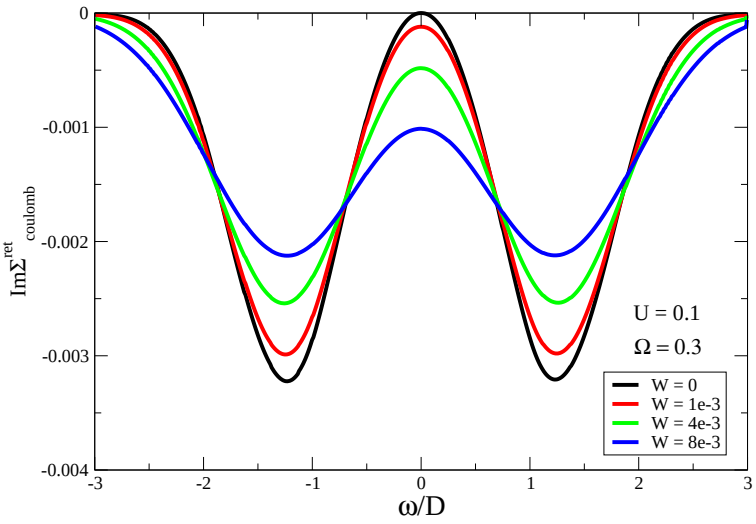

Figure 7.14: Electron retard self-energy from electron coulomb interaction

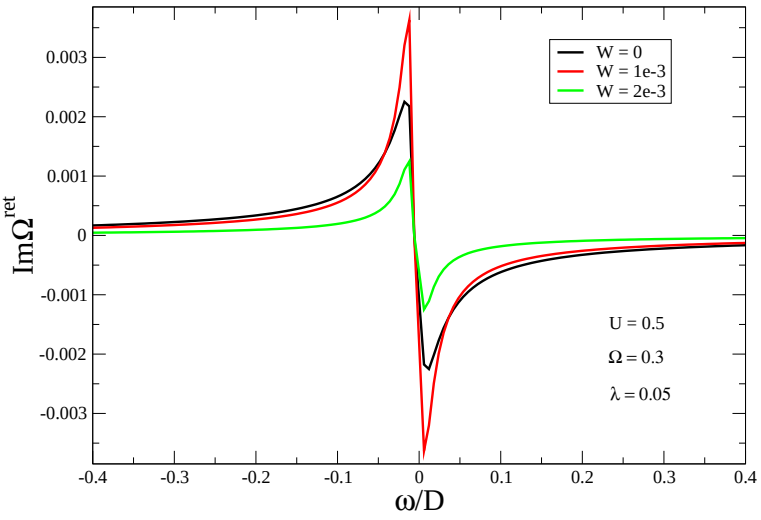

Figure 7.15: Photon retarded self-energy under different U

Chapter 8

Summary

In the beginning of this thesis, we have taken a overview on plasmon physics. Than we present the Keldysh Green's function, which has been employed to handle nonequilibrium problem.

In the previous chapters, we discussed the coupling an electron conduction band to a single laser mode. We treat the laser as second quantized photons. The coulomb interaction is also included in the model. The numerical results confirm that the coupled laser field arises fano resonance structure in the electron density of state. Laser pumps electrons from blow the fermi edge to above, but only those with $|\epsilon_p| < mode\, frequency$. Therefore, we can see in the distribution function harmonic stage, asymmetric to the fermi edge. On the other hand, over strong laser intensity might wash out the resonance effect.

The electron coulomb interaction diminishes the effect caused by the laser. As the coulomb interaction strength increases, either fano resonance in the electron DOS or harmonic effect in the electron distribution function will be extenuated.

Appendix A

Derivation of Dyson's Equation In Keldysh Space

The Derivation will follow the notation of Landau-Lifschitz Volume 10.

$$\bar{G} = \begin{pmatrix} 0 & G^A \\ G^R & F \end{pmatrix} \quad \bar{\Sigma} = \begin{pmatrix} \Omega & \Sigma^R \\ \Sigma^A & 0 \end{pmatrix}$$

where $F = G^> + G^<$ and $\Omega = \Sigma^{++} + \Sigma^{--} = -(\Sigma^> + \Sigma^<)$

The dyson equation has the form:

$$\bar{G}(\vec{p}, w) = \bar{G}_o(\vec{p}, w) + \bar{G}_o(\vec{p}, w)\bar{\Sigma}(\vec{p}, w)\bar{G}(\vec{p}, w)$$

For Convinience, we shall omit the arguments

$$\bar{G} = \bar{G}_o + \bar{G}_o\bar{\Sigma}\bar{G}$$

We do the matrix multiplication now:

$$\begin{pmatrix} 0 & G^A \\ G^R & F \end{pmatrix} = \begin{pmatrix} 0 & G_0^A \\ G_0^R & F_0 \end{pmatrix} + \begin{pmatrix} 0 & G_0^A \\ G_0^R & F_0 \end{pmatrix} \begin{pmatrix} \Omega & \Sigma^R \\ \Sigma^A & 0 \end{pmatrix} \begin{pmatrix} 0 & G^A \\ G^R & F \end{pmatrix}$$

Then we get:

$$\begin{pmatrix} 0 & G^A \\ G^R & F \end{pmatrix} = \begin{pmatrix} 0 & G_0^A \\ G_0^R & F_0 \end{pmatrix} + \begin{pmatrix} 0 & G_0^A\Sigma^A G^A \\ G_0^R\Sigma^R G^R & G_0^R\Omega G^a + F_0\Sigma^A G^A + G_0^R\Sigma^R F \end{pmatrix}$$

then we obtain the dyson equations for each component:

$$G^A = G_0^A + G_0^A\Sigma^A G^A \tag{A.1}$$

$$G^R = G_0^R + G_0^R \Sigma^R G^R \tag{A.2}$$

$$F = F_0 + G_0^R \Omega G^a + F_0 \Sigma^A G^A + G_0^R \Sigma^R F \tag{A.3}$$

Equations (1) and (2) are useful. We need to do some simplification to Equation (3).
According to the defination of Green's function, we have these relations: $F = G^< + G^>$ and $G^R - G^A = G^> - G^<$ from that we know

$$F = G^R - G^A + 2G^< \tag{A.4}$$

Similarly we have $\Omega = -(\Sigma^> + \Sigma^<)$ and $\Sigma^R - \Sigma^A = \Sigma^< - \Sigma^>$
Then we know

$$\Omega = \Sigma^R - \Sigma^A - 2\Sigma^< \tag{A.5}$$

Plug (4) and (5) into (3), we get:

$$\begin{aligned} G^R - G^A + 2G^< = {} & G_0^R - G_0^A + 2G_0^< + G_0^R(\Sigma^R - \Sigma^A - 2\Sigma^<)G^A \\ & + (G_0^R - G_0^A + 2G_0^<)\Sigma^A G^A + G_0^R \Sigma^R (G^R - G^A + 2G^<) \end{aligned} \tag{A.6}$$

Again using (1) and (2) to (6), we get:

$$G^< = G_0^< - G_0^R \Sigma^< G^A + G_0^< \Sigma^A G^A + G_0^R \Sigma^R G^<$$

$$\Longrightarrow (1 - G_0^R \Sigma^R) G^< = G_0^< (1 + \Sigma^A G^A) - G_0^R \Sigma^< G^A$$

$$\Longrightarrow G^< = (1 + \Sigma^R G^R) G_0^< (1 + \Sigma^A G^A) - G^R \Sigma^< G^A \tag{A.7}$$

Appendix B

Kramers-Kronig Relation

The Kramers-Kronig relations are related to mathematical properties of the function. It is useful when we need to know about the imaginary part of any complex function from it's real part or the other way around. In physiks, they are used to connect the real part and the imaginary part of response functions.

B.1 Derivation

Starting with the application of the residue theorem for complex integration, for any analytic function χ, which is analytic in the upper half plane, we have

$$\oint \frac{\chi(\omega')}{\omega' - \omega} d\omega' = 0 \tag{B.1}$$

The contour encloses the upper half plane at infinity, the real axis and a small half circle over the pole at $\omega = \omega'$, leaving no pole inside. So the evaluation of the integral is zero. After decompose the integral into contributions along each of the segments, there are only two terms that are non-zero. The segment at infinity vanishes with the assumption $\chi(\omega)$ vanishes as $|\omega| \to \infty$. Survived are the integrals along the real axis and the half-circle around the pole

$$\mathcal{P} \int_{-\infty}^{\infty} \frac{\chi(\omega')}{\omega' - \omega} d\omega' - i\pi\chi(\omega) = 0 \tag{B.2}$$

The second term on the left-hand side is obtained by using the theory of residues. Then we have the compact form of the Kramers-Kronig relations.

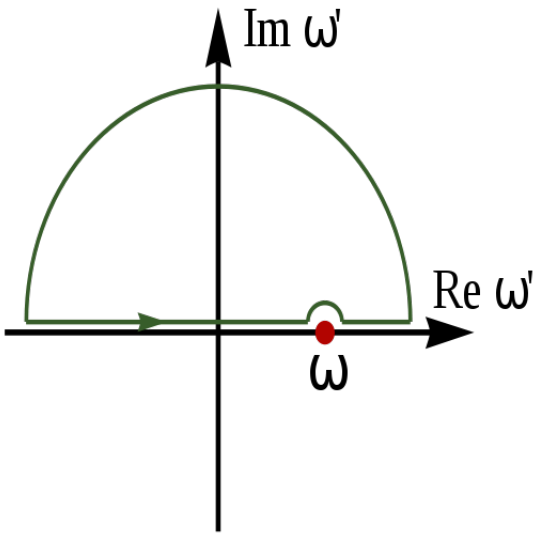

Figure B.1: Integral contour for deriving Kramers-Kronig relations

$$\chi(\omega) = \frac{1}{i\pi}\int_{-\infty}^{\infty}\frac{\chi(\omega')}{\omega'-\omega}d\omega' \tag{B.3}$$

With this simple relation, there comes the connection between the real and imaginary components. Let's define χ_1 and χ_2 to be the complex components of χ

$$\chi(\omega) = \chi_1(\omega) + i\chi_2(\omega) \tag{B.4}$$

Then from Eq.(B.3) we can solve

$$\chi_1(\omega) = \frac{1}{\pi}\mathcal{P}\int_{-\infty}^{\infty}\frac{\chi_2(\omega')}{\omega'-\omega} \tag{B.5}$$

$$\chi_2(\omega) = -\frac{1}{\pi}\mathcal{P}\int_{-\infty}^{\infty}\frac{\chi_1(\omega')}{\omega'-\omega} \tag{B.6}$$

The hypothesis one has to make about the complex function χ is analytic in the upper half-plane. This corresponds to the causality of retarded function. Therefore we can apply this relation to calculate the real part from the imaginary part of the selfenergy

$$\Re\Sigma^{ret}(\omega) = \frac{1}{\pi}\mathcal{P}\int_{-\infty}^{\infty}d\omega'\frac{\Im\Sigma^{ret}(\omega')}{\omega'-\omega} \tag{B.7}$$

The advanced functions are analytic in the lower half plane, they have a sign difference comparing to the retarded functions

$$\Re\Sigma^{adv}(\omega) = -\frac{1}{\pi}\mathcal{P}\int_{-\infty}^{\infty} d\omega' \frac{\Im\Sigma^{adv}(\omega')}{\omega' - \omega} \tag{B.8}$$

Appendix C

Green's Function for Noninteracting Particles

The real time Green's function for noninteracting particles can be found in almost all the textbook on many-particle physics. It it convenient to have it in the appendix.

C.1 Fermions

We start with the noninteracting fermions. The Hamiltonian is:

$$H_0 = \sum_{k\sigma} \xi_k c^\dagger_{k\sigma} c_{k\sigma} \tag{C.1}$$

where $\xi_k = \epsilon_k - \mu$ is the single-particle energy measured with respect to the chemical potential. $c_{k\sigma}$ and $c^\dagger_{k\sigma}$ are the fermion annihilation and creation operator. We are going to solve time dependency of the operator. In the Heisenberg picture, the time-evolution of the annihilation operator is

$$c_{k\sigma} = e^{iH_0 t/\hbar} c_{k\sigma} e^{-iH_0 t/\hbar} \tag{C.2}$$

We differentiate Eq.C2 with repect to t

$$\begin{aligned} i\hbar \frac{\partial}{\partial t} c_{k\sigma}(t) &= [c_{k\sigma}, H_0] \\ &= \xi_k c_{k\sigma} \end{aligned} \tag{C.3}$$

where we have used the relation

$$[A, BC] = \{A, B\}C - B\{A, C\} \tag{C.4}$$

and the usual fermion anticommutation relations

$$\{c_{k\sigma}, c_{k'\sigma'}\} = 0 \qquad \{c^\dagger_{k\sigma}, c^\dagger_{k'\sigma'}\} = 0 \tag{C.5}$$

$$\{c_{k\sigma}, c^\dagger_{k'\sigma'}\} = \delta_{k,k'}\delta_{\sigma,\sigma'} \tag{C.6}$$

Then Eq.C3 has the simple solution

$$c_{k\sigma}(t) = e^{-i\xi_t/\hbar}c_{k\sigma} \tag{C.7}$$

$c^\dagger$ is the hermitian conjugate of $c_{k\sigma}$

$$c^\dagger_{k\sigma}(t) = e^{i\xi_t/\hbar}c^\dagger_{k\sigma} \tag{C.8}$$

With the definition of Green's function, it is easy to calculate the unperturbed Green's function

$$\begin{aligned} G_0^{+-}(k\sigma t, k'\sigma' t') &= i\hbar^{-1}\langle c^\dagger_{k'\sigma'}(t')c_{k\sigma}(t)\rangle_0 \\ &= i\hbar^{-1}e^{-i\xi(t-t')/\hbar}\langle n_{k\sigma}\rangle\delta_{k,k'}\delta_{\sigma,\sigma'} \end{aligned} \tag{C.9}$$

$$\begin{aligned} G_0^{-+}(k\sigma t, k'\sigma' t') &= -i\hbar^{-1}\langle c_{k\sigma}(t)c^\dagger_{k'\sigma'}(t')\rangle_0 \\ &= -i\hbar^{-1}e^{-i\xi(t-t')/\hbar}[1 - \langle n_{k\sigma}]\rangle\delta_{k,k'}\delta_{\sigma,\sigma'} \end{aligned} \tag{C.10}$$

$$\begin{aligned} G_0^{ret}(k\sigma t, k'\sigma' t') &= -i\hbar^{-1}\theta(t-t')\langle c^\dagger_{k'\sigma'}, (t')c_{k\sigma}(t)\rangle_0 \\ &= -i\hbar^{-1}e^{-i\xi(t-t')/\hbar}\theta(t-t')\langle n_{k\sigma}\rangle_0\delta_{k,k'}\delta_{\sigma,\sigma'} \end{aligned} \tag{C.11}$$

$$\begin{aligned} G_0^{adv}(k\sigma t, k'\sigma' t') &= i\hbar^{-1}\theta(t'-t)\langle c^\dagger_{k'\sigma'}, (t')c_{k\sigma}(t)\rangle_0 \\ &= i\hbar^{-1}e^{-i\xi(t'-t)/\hbar}\theta(t-t')\langle n_{k\sigma}\rangle_0\delta_{k,k'}\delta_{\sigma,\sigma'} \end{aligned} \tag{C.12}$$

The Fourier transforms of the Green's functions are

$$G_0^{+-}(k\sigma, \omega) = 2\pi i\langle n_{k\sigma}\rangle\delta(\omega - \xi_k) \tag{C.13}$$

$$G_0^{-+}(k\sigma,\omega) = 2\pi i\{\langle n_{k\sigma}\rangle - 1\}\delta(\omega - \xi_k) \tag{C.14}$$

$$G_0^{ret}(k\sigma,\omega) = \frac{1}{\omega - \xi_k + i\eta} \tag{C.15}$$

$$G_0^{adv}(k\sigma,\omega) = \frac{1}{\omega - \xi_k - i\eta} \tag{C.16}$$

where $\eta = 0^+$. In thermal equilibrium case, the distribution funtion of fermion is the Fermi-Dirac distribution function

$$\langle n_\omega\rangle = n_F(\omega) = \frac{1}{e^{\beta\omega}+1} \qquad \beta = \frac{1}{k_B T} \tag{C.17}$$

We define the fermion spectral function $A_0(k\sigma,\omega)$ is defined as

$$A(k\sigma,\omega) = i[G^{ret}(k\sigma,\omega) - G^{adv}(k\sigma,\omega)] = -2\Im G^{ret}(k\sigma,\omega) \tag{C.18}$$

The spectral function fullfill the sum rule

$$\int_{-\infty}^{+\infty} \frac{d\omega}{2\pi} A(k\sigma,\omega) = 1 \tag{C.19}$$

For the noninteracting Green's function, we can write

$$G_0^{+-}(k\sigma,\omega) = i n_F(\omega) A_0(k\sigma,\omega) \tag{C.20}$$

$$G_0^{-+}(k\sigma,\omega) = i\{n_F(\omega) - 1\} A_0(k\sigma,\omega) \tag{C.21}$$

C.2 Bosons

The hamiltonian for single mode boson is

$$H_0 = \Omega_0\ a^\dagger a \tag{C.22}$$

where Ω_0 is the single mode frequency. a and $a^\dagger$ are the boson annihilation and creation operator. In Heisenberg picture, the time-evolution of the annihilation operator

$$a(t) = e^{iH_0 t/\hbar} a e^{-iH_0 t/\hbar} \tag{C.23}$$

the equation of motion to this operator is

$$i\hbar\frac{\partial}{\partial t}a(t) = [a, H_0] = \Omega_0 a(t) \tag{C.24}$$

where we have used the relation

$$[A, BC] = \{A, B\}C - B\{A, C\} \tag{C.25}$$

and the usual boson commutation relations

$$[a, a] = 0 \qquad [a^\dagger, a^\dagger] = 0 \tag{C.26}$$

$$[a, a^\dagger] = 1 \tag{C.27}$$

The $a(t)$ has the simple solution

$$a(t) = e^{-iH_0 t/\hbar}a \tag{C.28}$$

The creation operator is just the hermitian conjugate of a

$$a^\dagger(t) = e^{iH_0 t/\hbar}a^\dagger \tag{C.29}$$

The real-time single-particle Green's function for single mode boson are to be calculated according to the definition

$$\begin{aligned} D_0^{+-} &= -i\hbar^{-1}\langle[a^\dagger(t') + a(t')][a^\dagger(t) + a(t)]\rangle \\ &= -i\hbar^{-1}(\langle a^\dagger(t')a(t)\rangle_0 + \langle a(t')a(t)^\dagger\rangle_0 \\ &= -i\hbar^{-1}(e^{-i\Omega_0(t-t')/\hbar}\langle a^\dagger a\rangle_0 + e^{i\Omega_0(t-t')/\hbar}\langle aa^\dagger\rangle_0) \\ &= -i\hbar^{-1}(e^{-i\Omega_0(t-t')/\hbar}\langle n_0\rangle_0 + e^{i\Omega_0(t-t')/\hbar}[\langle n_0\rangle_0 + 1]) \end{aligned} \tag{C.30}$$

$$D_0^{-+} = D_0^{+-} \tag{C.31}$$

$$\begin{aligned} D^{ret}(t, t') &= -i\hbar^{-1}\theta(t - t')\langle[(a^\dagger(t) + a(t)), (a^\dagger(t') + a(t'))]\rangle_0 \\ &= -i\hbar^{-1}\theta(t - t')(\langle[(a^\dagger(t), a(t')]\rangle_0 + \langle[a(t), a^\dagger(t'))]\rangle_0) \\ &= i\hbar^{-1}\theta(t - t')(-e^{i\Omega_0(t-t')/\hbar} + e^{-i\Omega_0(t-t')/\hbar}) \end{aligned} \tag{C.32}$$

$$\begin{aligned} D^{adv}(t,t') &= i\hbar^{-1}\theta(t'-t)\langle[(a^\dagger(t)+a(t)),(a^\dagger(t')+a(t'))]\rangle_0 \\ &= i\hbar^{-1}\theta(t'-t)(\langle[(a^\dagger(t),a(t')]\rangle_0+\langle[a(t),a^\dagger(t'))]\rangle_0) \\ &= i\hbar^{-1}\theta(t'-t)(-e^{i\Omega_0(t-t')/\hbar}+e^{-i\Omega_0(t-t')/\hbar}) \end{aligned} \tag{C.33}$$

where $n_0 = a^\dagger a$. The Green's functions have the Fourier transforms

$$D_0^{+-}(\omega) = -2\pi i\{\langle n_0\rangle\delta(\omega-\Omega_0)+(\langle n_0\rangle+1)\delta(\omega+\Omega_0)\} \tag{C.34}$$

$$D_0^{-+}(\omega) = -2\pi i\{\langle n_0\rangle\delta(\omega+\Omega_0)+(\langle n_0\rangle+1)\delta(\omega-\Omega_0)\} \tag{C.35}$$

$$D^{ret} = \frac{1}{\omega-\Omega_0+i\eta}-\frac{1}{\omega+\Omega_0+i\eta} \qquad \eta = 0^+ \tag{C.36}$$

$$D^{adv} = \frac{1}{\omega-\Omega_0-i\eta}-\frac{1}{\omega+\Omega_0-i\eta} \qquad \eta = 0^+ \tag{C.37}$$

In a thermal equilibrium, the distribution function is the Bose-Einstein distribution

$$\langle n_0\rangle = n_B(\Omega_0) = \frac{1}{e^{\beta\Omega_0}-1} \tag{C.38}$$

The boson spectral function is defined in a similar way as for fermion

$$B(\omega) = i[D^{ret}(\omega)-D^{adv}(\omega)] = -2\Im[D^{ret}(\omega)] \tag{C.39}$$

with the sum rule

$$\int_{-\infty}^{+\infty}\frac{d\omega}{2\pi}B(\omega) = 0 \tag{C.40}$$

List of Figures

Bibliography

[1] Stefan Maier. *Plasmonics:Fundamentals and Applications.* Springer (2007).

[2] Atwater Harry. *The Promise of Plasmonics.* Scientific American **296**(4): 56-63.

[3] J. R. Krenn, J. C. Weeber, *Surface plasmon polaritons in metal stripes and wires* Philos. Trans. R. Soc. London Ser. A **362**, 739 (2004)

[4] W. L. Barnes, A. Dereux, and T. W. Ebbesen, *Surface plasmon subwavelength optics* Nature(London) **424**, 824 (2003)

[5] H.J.Lezec et al., *Beaming Light from a Subwavelength Aperture* Science **297**, 820 (2002).

[6] Ozbay,Ekmel. *Plasmonics:Meeting Photonics and Electronics at Nanoscale Dimensions* Science **311**(5758): 189-193.

[7] S. Nakamura, G. Fasol, *The Blue Laser Diode: GaN-Based Light Emitting Diode and Lasers* Springer, Berlin, 1997

[8] J. Vuckovic, M. Loncar, A. Scherer, *Surface plasmon enhanced light-emitting diode* IEEE J.Quant.Electr. **36**, 1131 (2000).

[9] S. G. Tikhodeev, N. A. Gippius , A.Christ , T. Zentgraf, J. Kuhl, H. Giessen, *Waveguide-plasmon polaritons in photonic crystal slabs with metal nanowires*, Phys. stat. sol. (c) **2**, 795 (2005).

[10] L. C. Andreani, D. Gerace, *Light-matter interaction in photonic crystal slabs* Phys. stat. sol. (b) **244**, 3528 (2007).

[11] J. B. Masson, A. Podzorov, and G. Gallot, *Extended Fano model of Extraordinary Electromagnetic Transmission through subwavelength hole arrays in the terahertz domain.* Opt. Express, Vol. **17**, 15280 (2009)

[12] H. Liu, P. Lalanne *Microscopic theory of the extraordinary optical transmission.* Nature **452**, 728 (2008)

[13] H. Raether. *Surface Plasmons*. Spriner, Berlin, 1988.

[14] Heinz Raether. *Excitation of plasmons and interband transitions by electrons.* Springer-Verlag (1980).

[15] Stefan Maier at el. *Plasmonics: Localization and guiding of electromagnetic energy in metal/dielectric structures*. Appl Phys. **98**, 011101 (2005).

[16] A. Manjavacas and F. J. Garcia de Abajo, *Robust plasmon waveguides in strongly-interacting nanowire arrays*, arXiv:**0806**.1881v1

[17] J .B. Pendry, *Negative Refraction Makes a Perfect Lens*. Phys. Rev. Lett. **85**, 3966 (2000).

[18] N. Fang, H. Lee, C. Sun, X. Zheng, *Sub Diffraction-Limited Optical Imaging with a Silver Superlens* Science **308**, 534 (2005)

[19] A. Christ, S. G. Tikhodeev, N. A. Gippius, J. Kuhl, H. Giessen. *Waveguide Plasmon Polaritons: Strong Coupling of Photonic and Electronic Resonances in a Metallic Photonic Crystal Slab* Phys. Rev. Lett **91** 183901, 2003

[20] P. M. Platzman and P. Eisenberger, *Presence of an Incipient Wigner Electron Lattice in Solid-State Electron Gases*, Phys. Rev. Lett. **33**, 152 (1974).

[21] C. H. Chen, A. E. Meixner, and B. M. Kincaid, *Bulk Plasmon Dispersion in Si for* $0 < q < 1.5qF$, Phys. Rev.Lett. **44**, 951 (1980).

[22] F. Green, D. N. Lowy, and J. Szymanski, *Direct Evidence for Dynamic Electron-Electron Coulomb Correlations in Metals*, Phys. Rev. Lett. **48**, 638 (1982)

[23] F. Green, D. Neilson, and J. Szymanski, *Dynamic structure factor for the electron gas in metallic systems*, Phys. Rev. B **31**, 2796 (1985).

[24] K. Sturm, W. Schülke and J. R. Schmitz *Plasmon-Fano resonance inside the particle-hole excitation spectrum of simple metals and semiconductors.* Phys. Rev. Lett. **68**, 228, (1992)

[25] A. V. Zayats, I. I. Smolyaninov, and A. A. Maradudin, *Nano-optics of surface plasmon polaritons* , Phys. Rep. **408**, 131 (2005).

[26] F. J. Garcia de Abajo, *Colloquium: Light scattering by particle and hole arrays*, Rev. Mod. Phys. **79**, 1267 (2007)

[27] C. Genet and T. W. Ebbesen, *Light in tiny holes* , Nature (London) **445**, 39 (2007)

[28] T. V. Teperik, and A. G. Borisov, *Optical resonances in the scattering of light from a nanostructured metal surface: A three-dimensional numerical study.* Phys. Rev. B **79**, 245409 (2009)

[29] T. W. Ebbesen, H. J. Lezec, H. F. Ghaemi, T. Thiol, and P. A. Wolff, *Extraordinary optical transmission through sub-wavelength hole arrays*, Nature (London) **391**, 667 (1998)

[30] J. A. Porto, F. J. Garcia-Vidal, and J. B. Pendry, *Transmission Resonances on Metallic Gratings with Very Narrow Slits*, Phys. Rev. Lett. **83**,2845 (1999).

[31] M. M. J. Treacy, *Dynamical diffraction explanation of the anomalous transmission of light through metallic gratings* , Phys. Rev. B **66**, 195105 (2002)

[32] F. Yang and J. R. Sambles, *Resonant Transmission of Microwaves through a Narrow Metallic Slit* Phys. Rev. Lett. **89**, 063901 (2002).

[33] S. A. Darmanyan and A. V. Zayats, *Light tunneling via resonant surface plasmon polariton states and the enhanced transmission of periodically nanostructured metal films. An analytical study* , Phys. Rev. B **67**, 035424 (2003).

[34] F. J. Garcia de Abajo and J. J. Saenz, *Electromagnetic Surface Modes in Structured Perfect-Conductor Surfaces* , Phys. Rev. Lett. **95**, 233901 (2005).

[35] D. Pacifici, H. J. Lezec, L. A. Sweatlock, R. J. Walters, and H. A. Atwater, *Universal optical transmission features in periodic and quasiperiodic hole arrays*, Opt. Express **16**, 9222 (2008).

[36] H. Liu and P. Lalanne, *Microscopic theory of the extraordinary optical transmission*, Nature (London) **452**, 782 (2008)

[37] U. Schroter and D. Heitmann, *Surface-plasmon-enhanced transmission through metallic gratings* , Phys. Rev. B **58**, 15419 (1998).

[38] H. E. Went, A. P. Hibbins, J. R. Sambles, C. R. Lawrence, and A. P. Crick, *Selective transmission through very deep zero-order metallic gratings at microwave frequencies*, Appl. Phys. Lett. **77**, 2789 (2000).

[39] Q.Cao and P. Lalanne, *Negative Role of Surface Plasmons in the Transmission of Metallic Gratings with Very Narrow Slits*, Phys, Rev. Lett. **88**, 057403 (2002).

[40] F. Marquier, J.J. Greffet, S. Collin, F. Pardo, and J. L. Pelouard, *Resonant transmission through a metallic film due to coupled modes*, Opt. Express **13**, 70 (2005).

[41] M. C. Hutley and D. Maystre, *The total absorption of light by a diffraction grating*, Opt. Commun. **19**, 431 (1976).

[42] E. Popov, L. Tsonev, and D. Maystre, *Lamellar metallic grating anomalies*, Appl. Opt. **33**, 5214 (1994).

[43] W. C. Tan, J. R. Sambles, and T. W. Preist, *Double period zero order metal gratings as effective selective absorbers*, Phys. Rev. B **61**, 13177 (2000).

[44] S. Collin, F. Pardo, R. Teissier, and J. L. Pelouard, Appl. *Efficient light absorption in metal semiconductor metal nanostructures*, Phys. Lett. **85**, 194 (2004).

[45] N. Bonod, G. Tayeb, D. Maystre, S. Enoch, and E. Popov, *Total absorption of light by lamellar metallic gratings*, Opt. Express **16**, 15431 (2008).

[46] M. Laroche, C. Arnold, F. Marquier, R. Carminati, J. J. Greffet, S. Collin, N. Bardou, and J. L. Pelouard, *Highly directional radiation generated by a tungsten thermal source* , Opt. Lett. **30**, 2623 (2005).

[47] Y. De Wilde, F. Formanek, R. Carminati, B. Gralak, P.A. Lemoine, K. Joulain, J. P. Mulet, Y. Chen, and J. J. Greffet, *Thermal radiation scanning tunnelling microscopy*, Nature (London) **444**, 740 (2006).

[48] G. Biener, N. Dahan, A. Niv, V. Kleiner, and E. Hasmana, *Highly coherent thermal emission obtained by plasmonic bandgap structures*, Appl. Phys. Lett. **92**, 081913 (2008).

[49] C. Jiang, K. Kempa, J. Zhao, U. Schlecht, U. Kolb, T. Basche, M. Burghard, and A. Mews, *Strong enhancement of the Breit-Wigner-Fano Raman line in carbon nanotube bundles caused by plasmon band formation.* Phys. Rev. B **66**, 161404, (2002)

[50] S. Iijima, *Helical microtubules of graphitic carbon*, Nature (London) **354**, 56 (1991)

[51] R. Saito, G. Dresselhaus, and M. S. Dresselhaus, *Physical Properties of Carbon Nanotubes*, Imperial College Press, London, (1998).

[52] H. W. C. Postma, T. Teepen, Z. Yao, M. Grifoni, and C. Dekker, *Carbon Nanotube Single-Electron Transistors at Room Temperature* , Science **293**, 76 (2001).

[53] J. Kong, N. R. Franklin, C. Zhou, M. G. Chapline, S. Peng, K. Cho, and H. Dai, *Nanotube Molecular Wires as Chemical Sensors* , Science **287**, 622 (2000).

[54] W.L. Barnes, T.W. Preist, S.C. Kitson, and J.R. Sambles, *Physical origin of photonic energy gaps in the propagation of surface plasmons on gratings*, Phys. Rev. B **54**, 6227-6242 (1996).

[55] I. Avrutsky, Y. Zhao, and V. Kochergin, *Surf ace-plasmon-assisted resonant tunneling of light through a periodically corrugated thin metal film* , Optics Letters **25**, 595-597 (2000).

[56] T. Ito and K. Sakoda, *Photonic bands of metallic systems. II. Features of surface plasmon polaritons*, Phys. Rev. B **64**, 045117 (2001)

[57] F.J. Garca-Vidal and L. Martn-Moreno, *Transmission and focusing of light in one-dimensional periodically nanostructured metals*, Phys. Rev. B **66**, 155412 (2002).

[58] J. B. Pendry, L. Martn-Moreno, and F. J. Garca-Vidal, *Mimicking surface plasmons with structured surfaces*, Science **305**, 847-848 (2004).

[59] C. Ropers, D.J. Park, G. Stibenz, G. Steinmeyer, J. Kim, D.S. Kim, and C. Lienau, *Femtosecond light transmission and subradiant damping in plasmonic crystals*, Phys. Rev. Lett. **94**, 113901 (2005).

[60] A. Christ, T. Zentgraf, J. Kuhl, S.G. Tikhodeev, N.A. Gippius, and H. Giessen, *Optical properties of planar metallic photonic crystal structures: Experiment and theory*, Phys. Rev. B **70**, 125113 (2004).

[61] A. Christ, S.G. Tikhodeev, N.A. Gippius, J. Kuhl, and H. Giessen, *Waveguide plasmon polaritons: Strong coupling of photonic and electronic resonances in a metallic photonic crystal slab*, Phys. Rev. Lett. **91**, 183901 (2003).

[62] S. Coyle, M.C. Netti, J.J. Baumberg, M.A. Ghanem, P.R. Birkin, P.N. Bartlett, and D.M. Whittaker, *Confined plasmons in metallic nanocavities*, Phys. Rev. Lett. **87**, 176801 (2001).

[63] O.D. Velev, P.M. Tessier, A.M. Lenhoff, and E.W. Kaler, *A class of porous metallic nanostructures*, Nature **401**, 548 (1999).

[64] J.E.G.J.Wijnhoven, S.J.M. Zevenhuizen, M.A. Hendriks, D. Vanmaekelbergh, J.J. Kelly, and W.L. Vos, *Electrochemical assembly of ordered macropores in gold*, Adv. Mater. **12**, 888-890, 2000.

[65] N. Stefanou, A. Modinos, and V. Yannopapas, *Optical transparency of mesoporous metals*, Solid State Commun. **118**, 69-73 (2001).

[66] T.V. Teperik, V.V. Popov, and F.J. Garca de Abajo, *Void plasmons and total absorption of light in nanoporous metallic films*, Phys. Rev. B **71**, 085408 (2005).

[67] Petra Schmidt, Diplomarbeit, Physikalisches Institut, University Bonn (1999)

[68] T. V. Teperik, V. V. Popov, F. J. Garcia de Abajo, M. Abdelsalam, P. N. Bartlett, T. A. Kelf, Y. Sugawara, and J. J. Baumberg, *Strong coupling of light to flat metals via a buried nanovoid lattice: the interplay of localized and free plasmons.* Opt. Express **14**, 1965 (2006).

[69] A. Christ, G. Leveque, O.J.F. Martin, T. Zentgraf, J. Kuhl, C. Bauer, H. Giessen, and S.G. Tikhodeev, *Near-field induced tunability of surface plasmon polaritons in composite metallic nanostructures* Journal of Microscopy **229**, 344, (2008).

[70] T. J. Thompson, G. Rempe, and H. J. Kimble, *Observation of normal-mode splitting for an atom in an optical cavity*, Phys. Rev. Lett. 68, 1132 (1992).

[71] E. M. Purcell, *Spontaneous emission probabilities at radio frequencies*, Phys. Rev. **69** , 681 (1946).

[72] T. Yoshie et al., *Vacuum Rabi splitting with a single quantum dot in a photonic crystal nanocavity*, Nature (London) **432**, 200 (2004).

[73] C. Weisbuch, M. Nishioka, A. Ishikawa, and Y. Arakawa, *Observation of the coupled exciton-photon mode splitting in a semiconductor quantum microcavity*, Phys. Rev. Lett. **69** , 3314 (1992).

[74] J. M. Gerard et al., *Enhanced Spontaneous Emission by Quantum Boxes in a Monolithic Optical Microcavity*, Phys. Rev. Lett. **81** , 1110 (1998)

[75] P. Vasa, R. Pomraenke, S. Schwieger, Yu. I. Mazur, Vas. Kunets, P. Srinivasan, E. Johnson, J. E. Kihm, D. S. Kim, E. Runge, G. Salamo, and C. Lienau, *Coherent Exciton-Surface-Plasmon-Polariton Interaction in Hybrid Metal-Semiconductor Nanostructures.* Phys. Rev. Let. **101**, 116801, (2008).

[76] L. D. Landau and E. M. Lifschitz, *Course of Theoretical Physics, Volume 3*.

[77] N. Nagaosa, *Quantum Field Theory in Condensed Matter Physics*, Springer, 1995.

[78] A. Fetter and J. D. Walecka, *Quantum Theory of Many-Particle Systems*, Dover Publications,Inc, Mineola,N.Y., 2003.

[79] G. D. Mahan, *Many-Particle Physics*, Plenum Press, New York, 3rd Edition.

[80] J.W.Negele and H.Orland, *Quantum Many-Particle Systems*, Perseus Publishing, 1998.

[81] P. C. Martin and J. Schwinger, *Theory of Many-Particle Systems. I* , Phys. Rev, **115**:1342, 1959.

[82] J. Schwinger, Journ. Math. Phys. **2**(3):406, 1961.

[83] L. V. Keldysh, Sov. Phys. JETP, **20**(4):1018, 1965.

[84] L. P. Kadanoff and G. Baym. *Quantum Statistical Mechanics*, Benjamin, New York, 1962.

[85] J. Rammer and H . Smith. *Quantum field-theoretical methods in transport theory of metals*. Rev. Mod. Phys. **58**(1):323, 1986.

[86] K. N. Pathak. *Theory of Anharmonic Crystals* Physical Review. **139** , 1569. 1965

[87] I. J. Lalovf and K. T. Stoychev, *Nonlinear response function in case of polariton Fermi resonance.* J. Phys. C: Solid State Phys. **18**, 6691, (1985).

[88] S. De Liberato, and C. Ciuti, *Quantum theory of electron tunneling into intersubband cavity polariton states.* Phys. Rev. B **79**, 075317, (2009).

[89] L. I. Deych, A. Yamilov, and A. A. Lisyansky, *Local polariton modes and resonant tunneling of electromagnetic waves through periodic Bragg multiple quantum well structures.* Phys. Rev. B **64**, 075321, (2001).

[90] X. Wu, D. Li, W.-H. Sun, F. Gao, Z.-J. Zhang, and R.-W. Peng *Coupling of Terahertz Surface Plasmon Polaritons in Corrugated Stacks of Dielectric and Semiconductor* PIERS ONLINE, VOL. **5**, 101, (2009)

[91] I. R. Hooper and J. R. Sambles, *Surface plasmon polaritons on thin-slab metal gratings.* Phys. Rev. B **67**, 235404, (2003).

[92] M. Yamashita and M. Tsuji, *Simple Theory for Surface-Plasmon-Polariton Resonance on Sinusoidal Metal Surface: Application to SERS.* J. Phys. Soc. Jpn. **52**,2462, (1983).

[93] A. Quattropani and W. Czaja, *Quantum Theory of Exciton-Polaritons with Spatial Dispersion.* Physica Scripta **T29**, 162, (1989).

[94] J. M. Pitarke, V. M. Silkin, E. V. Chulkov, and P. M. Echenique, *Theory of surface plasmons and surface-plasmon polaritons.* Rep. Prog. Phys. **70**, 1, (2007).

[95] I. G. Breukelaar, *Surface Plasmon-Polaritons in Thin Metal Strips and Slabs: Waveguiding and Mode Cutoff.* Master Thesis, University of Ottawa, (2004).

[96] Z. Liu, M. D. Thoreson, A. V. Kildishev, and V. M. Shalaev, *Translation of nanoantenna hot spots by a metal-dielectric composite superlens* Appl. Phys. Lett. **95**, 033114, (2009).